

## RESEARCH ARTICLE

# Pacsin 2-dependent N-cadherin internalization regulates the migration behaviour of malignant cancer cells

Haymar Wint<sup>1</sup>, Jianzhen Li<sup>1,2</sup>, Tadashi Abe<sup>1</sup>, Hiroshi Yamada<sup>1</sup>, Takumi Higaki<sup>3,4</sup>, Yasutomo Nasu<sup>5</sup>, Masami Watanabe<sup>5</sup>, Kohji Takei<sup>1,\*</sup> and Tetsuya Takeda<sup>1,\*</sup>

## ABSTRACT

Collective cell migration is the coordinated movement of multiple cells connected by cadherin-based adherens junctions and is essential for physiological and pathological processes. Cadherins undergo dynamic intracellular trafficking, and their surface level is determined by a balance between endocytosis, recycling and degradation. However, the regulatory mechanism of cadherin turnover in collective cell migration remains elusive. In this study, we show that the Bin/amphiphysin/Rvs (BAR) domain protein pacsin 2 (protein kinase C and casein kinase substrate in neurons protein 2) plays an essential role in collective cell migration by regulating N-cadherin (also known as CDH2) endocytosis in human cancer cells. Pacsin 2-depleted cells formed cell–cell contacts enriched with N-cadherin and migrated in a directed manner. Furthermore, pacsin 2-depleted cells showed attenuated internalization of N-cadherin from the cell surface. Interestingly, GST pull-down assays demonstrated that the pacsin 2 SH3 domain binds to the cytoplasmic region of N-cadherin, and expression of an N-cadherin mutant defective in binding to pacsin 2 phenocopied pacsin 2 RNAi cells both in cell contact formation and N-cadherin endocytosis. These data support new insights into a novel endocytic route of N-cadherin in collective cell migration, highlighting pacsin 2 as a possible therapeutic target for cancer metastasis.

**KEY WORDS:** N-cadherin, Pacsin 2, Dynamin 2, Endocytosis, Collective cell migration

## INTRODUCTION


Cell migration is fundamental for diverse physiological and pathological processes, including development, immune responses and cancer metastasis (Yamada and Sixt, 2019). Cancer cells migrate either individually or collectively during metastasis (Pandya et al., 2017). Collectively migrating cancer cells are generally more

aggressive and resistant to chemotherapies compared to individually migrating cancer cells (Aceto et al., 2014). Collective cell migration is a coordinated movement of a group of cells that are connected via adherens junctions (Friedl and Gilmour, 2009; Rørth, 2009). Different guidance mechanisms, such as chemotaxis, haptotaxis, durotaxis and strain-induced mechanosensing, are involved in the collective movement of cells (Haeger et al., 2015; Shellard and Mayor, 2021). For successful collective cell migration, two groups of cell adhesion molecules play essential roles in generating and coordinating mechanical forces among cells: focal adhesion (FA) molecules such as integrins, which transmit forces between cells and the underlying extracellular matrix (ECM), and adherens junction molecules such as cadherins, which transmit forces at intercellular adhesion sites (Halbleib and Nelson, 2006; Ray et al., 2017).

Cadherins are homophilic  $Ca^{2+}$ -dependent cell adhesion molecules that play important roles in various physiological and pathological processes such as development (Gumbiner, 2005; Halbleib and Nelson, 2006) and cancer (Kaszak et al., 2020). There are over 100 different cadherin subtypes in vertebrates, and they can be classified into four groups: classical cadherins, desmosomal cadherins, protocadherins and unconventional cadherins (Yagi and Takeichi, 2000). From N- to C-terminus, each cadherin contains a large extracellular ectodomain followed by a transmembrane domain and a small cytoplasmic domain (Oda and Takeichi, 2011). Interactions between the ectodomains of cadherins from apposed cells mediate cell–cell contact, whereas the cytoplasmic domain contributes to linking cadherins to the underlying actin cytoskeleton by forming a complex with  $\alpha$ - and  $\beta$ -catenins (Ratheesh and Yap, 2012). The cytoplasmic domain of cadherins also binds to p120 catenin (hereafter referred to as p120; also known as CTNND1), which controls endocytosis and turnover of cadherin, thus regulating cell surface cadherin levels responsible for cell–cell adhesion (Cadwell et al., 2016). A recent study has shown that classical cadherins – E-cadherin (also known as CDH1) and N-cadherin (also known as CDH2) – mediate cell–cell contacts to enhance the spreading efficiency of collectively migrating cells (Zisis et al., 2022). Another study on collectively migrating endothelial cells has shown that polarized membrane protrusions enriched with unconventional VE-cadherin (CDH5) called ‘cadherin fingers’ serve as guidance cues that direct collective cell migration (Hayer et al., 2016). Furthermore, classical P-cadherin (CDH3) enhances the collective cell migration of myoblasts by activating Cdc42, increasing the strength and anisotropy of mechanical forces (Plutoni et al., 2016). The cadherin-mediated cell–cell contact is determined by a balance between endocytosis, recycling and degradation (Akhtar and Hotchin, 2001; Cadwell et al., 2016; Kowalczyk and Nanes, 2012; Le et al., 1999). However, the regulatory mechanisms of cadherin turnover in collective cell migration remain to be elucidated.

<sup>1</sup>Department of Neuroscience, Okayama University Graduate School of Medicine, Dentistry and Pharmaceutical Sciences, Shikata-cho 2-5-1, Kita-ku, Okayama 700-8558, Japan. <sup>2</sup>Laboratory for Neural Cell Dynamics, RIKEN Center for Brain Science, Hirosawa 2-1, Wako, Saitama 351-0198, Japan. <sup>3</sup>Faculty of Advanced Science and Technology, Kumamoto University, Kurokami, Chuo-ku, Kumamoto 860-8555, Japan. <sup>4</sup>International Research Organization for Advanced Science and Technology, Kumamoto University, Kurokami, Chuo-ku, Kumamoto 860-8555, Japan. <sup>5</sup>Department of Urology, Okayama University Graduate School of Medicine, Dentistry and Pharmaceutical Sciences, Okayama 700-8558, Japan.

\*Authors for correspondence (kohji@md.okayama-u.ac.jp; ttakeda@okayama-u.ac.jp)

 H.W., 0000-0002-2923-878X; J.L., 0000-0002-0580-2606; T.H., 0000-0002-1379-3930; K.T., 0000-0002-6555-9425; T.T., 0000-0002-3183-6551

This is an Open Access article distributed under the terms of the Creative Commons Attribution License (<https://creativecommons.org/licenses/by/4.0>), which permits unrestricted use, distribution and reproduction in any medium provided that the original work is properly attributed

Handling Editor: Michael Way  
Received 22 November 2022; Accepted 13 April 2023

Bin/amphiphysin/Rvs (BAR) domain proteins are a conserved family of proteins that possess the ability to sense membrane curvature and deform membranes (Peter et al., 2004; Safari and Suetsugu, 2012). BAR domain proteins play crucial roles in endocytosis (Takei et al., 1999), exocytosis (Pinheiro et al., 2014), cell migration (Sánchez-Barrena et al., 2012), cytokinesis (Takeda et al., 2013) and cancer metastasis (Yamamoto et al., 2011). BAR domains form ‘crescent-shaped’ dimers that are classified into three subtypes, each with distinctive topology and curvature: N-BAR (N-terminal amphipathic helix and BAR), F-BAR (Fes/CIP4 homology BAR) and I-BAR (inverse BAR) (Qualmann et al., 2011; Safari and Suetsugu, 2012). Pacsin (protein kinase C and casein kinase substrate in neurons protein; also known as synaptic dynamin-associated protein, syndapin) contains an F-BAR domain and an SH3 domain in its N- and C-termini, respectively (Dumont and Lehtonen, 2022). Three pacsin isoforms are expressed in mammalian cells: the neuronal isoform pacsin 1, the muscle-specific isoform pacsin 3 and the ubiquitously expressed isoform pacsin 2 (Modregger et al., 2000). Pacsin 2 has been implicated in caveolar endocytosis, vesicle trafficking and actin dynamics (Chandrasekaran et al., 2016; de Kreuk et al., 2011; Hansen et al., 2011; Senju et al., 2011). Pacsin 2 is also involved in the regulation of cell spreading and migration by associating with Rac1 (de Kreuk et al., 2011). Furthermore, based on TCGA PanCancer Atlas studies in cBioPortal (<https://www.cbioportal.org/>), deep deletions or mutations in the pacsin 2 gene that potentially cause gain or loss of function have been identified in samples from people with bladder cancer as well as other types of malignant cancers including ovarian and breast cancers (Cerami et al., 2012; Gao et al., 2013). Previous studies have shown that dynamin 2, a major pacsin 2-associated protein, is required for the internalization of E-cadherin (Miyashita and Ozawa, 2007; Paterson et al., 2003) and VE-cadherins (Chiasson et al., 2009). However, the requirement of pacsins in cadherin turnover remains elusive.

In this study, we show that pacsin 2 is involved in the collective cell migration of cancer cells by controlling N-cadherin internalization. Depletion of pacsin 2 in T24 bladder cancer cells and H1299 lung cancer cells induces cell–cell contacts enriched with N-cadherin. Electron microscopy shows that the cell–cell contacts induced by pacsin 2 depletion consist of interdigitating finger-like membranous protrusions. Imaging analyses of wound healing assays demonstrate that pacsin 2-depleted T24 cells exhibit directed cell migration. Furthermore, cell surface biotinylation and endocytosis assays show that N-cadherin internalization is inhibited in pacsin 2-depleted T24 cells. Interestingly, GST pull-down assays show that the SH3 domain of pacsin 2 binds to the cytoplasmic domain of N-cadherin, suggesting a direct role of pacsin 2 in regulating N-cadherin endocytosis. Indeed, expression of an N-cadherin mutant with defective pacsin 2 binding induced cell–cell contact formation and attenuated internalization, phenocopying pacsin 2 RNAi cells. These results suggest that pacsin 2 plays an essential role in regulating the endocytosis of N-cadherin, which affects the cell migration behaviour of malignant cancer cells.

## RESULTS

### Pacsin 2 localizes at the cell periphery in T24 cells

To determine the functions of pacsins in cancer cells, the expression and localization profiles of pacsin isoforms were examined in T24 cells. Immunoblot analysis of whole-cell extract from T24 cells revealed that all the pacsin isoforms were expressed in T24 cells (Fig. 1A). Immunofluorescence microscopy showed that pacsin 2 was concentrated at the cell periphery in T24 cells, whereas pacsin 1

and pacsin 3 dispersedly localized in the cytoplasm (Fig. 1B). Pacsin 2 interacts with dynamin 2, which is required for the formation of invadopodia in T24 cells (Zhang et al., 2016). However, pacsin 2 did not colocalize with dynamin 2 at the perinuclear invadopodia, but the two proteins did colocalize at the cell periphery (Fig. 1C). Similarly, pacsin 2 also colocalized with the essential actin organizer cortactin (CTTN) at the cell periphery, but they were not colocalized at invadopodia (Fig. 1C). Furthermore, a degradation assay using FITC–gelatin confirmed that pacsin 2 does not localize to the degradation-competent invadopodia in perinuclear regions (Fig. 1D). These results suggest that, unlike dynamin 2, pacsin 2 is not involved in invadopodia formation but instead plays a role in processes at the cell periphery, such as cell migration.

### Pacsin 2 depletion induces directional migration of T24 cells

To elucidate whether pacsin 2 is involved in the migration of T24 cells, the effect of pacsin 2 depletion was examined in a wound healing assay. Control RNAi T24 cells (treated with a non-targeting siRNA, siCtrl) migrated slowly, and only 15.7% of the scratched area was filled after 12 h (Fig. 2A,B, siCtrl). In contrast, pacsin 2 RNAi cells showed enhanced migration activity, and the wound closure area was extended to 31.3–54.1% in 12 h (Fig. 2A,B, siPacsin 2 #1, #2 and #3). Immunoblot analyses confirmed that all three different siRNAs targeting pacsin 2 caused depletion of pacsin 2 (Fig. 2C). These results suggest that pacsin 2 negatively regulates cell migration activities of T24 cells.

To clarify the cause of the enhanced cell migration exhibited by pacsin 2 RNAi cells, the dynamics of cell migration were analysed by live-cell imaging in the wound healing assay. Tracking of representative cells showed that control RNAi cells moved with an average speed of 4.1  $\mu\text{m}/\text{min}$ , but they moved randomly (Fig. 2D–G, siCtrl; Movie 1). In contrast, pacsin 2 RNAi cells migrated in a more directed manner, though their speed was comparable to that of control RNAi cells (3.5  $\mu\text{m}/\text{min}$ ) (Fig. 2D–G, siPacsin 2; Movie 2). These results suggest that pacsin 2 has a role in regulating the directionality of cell migration.

### Pacsin 2 depletion induces cell–cell contacts enriched with N-cadherin

To elucidate how pacsin 2 can affect the directionality of cell migration, cellular phenotypes were analysed using immunofluorescence microscopy. Control RNAi cells tended to grow individually, and only 34.5% of cells formed cell–cell contacts at subconfluent cell densities (Fig. 3A,B, siCtrl). In contrast, pacsin 2 RNAi induced cell clustering, and more than 77.5% of cells exhibited cell–cell contacts (Fig. 3A,B, siPacsin 2 #1, #2 and #3). Similarly, cell cluster formation was also induced by dynamin 2 RNAi (55.3%), whereas only 26.4% of control RNAi cells exhibited cell–cell contacts (Fig. S1A,B). These results suggest that pacsin 2 and dynamin 2 are involved in the formation of cell–cell contacts in T24 cells.

To identify the molecular components of the cell–cell contacts induced following RNAi of pacsin 2 or dynamin 2, the expression and localization profiles of cadherins were examined. Immunoblot analyses showed that T24 cells, which represent papillary bladder carcinoma, expressed E-cadherin but not N-cadherin, whereas T24 cells, which represent more aggressive bladder cancer, expressed N-cadherin but not E-cadherin (Fig. S2A). In contrast, neither classical P-cadherin nor unconventional VE-cadherin were expressed in T24 cells (Fig. S2A). To determine whether N-cadherin is a component of the cell–cell contacts induced following RNAi of pacsin 2 or dynamin 2, the localization of N-cadherin in

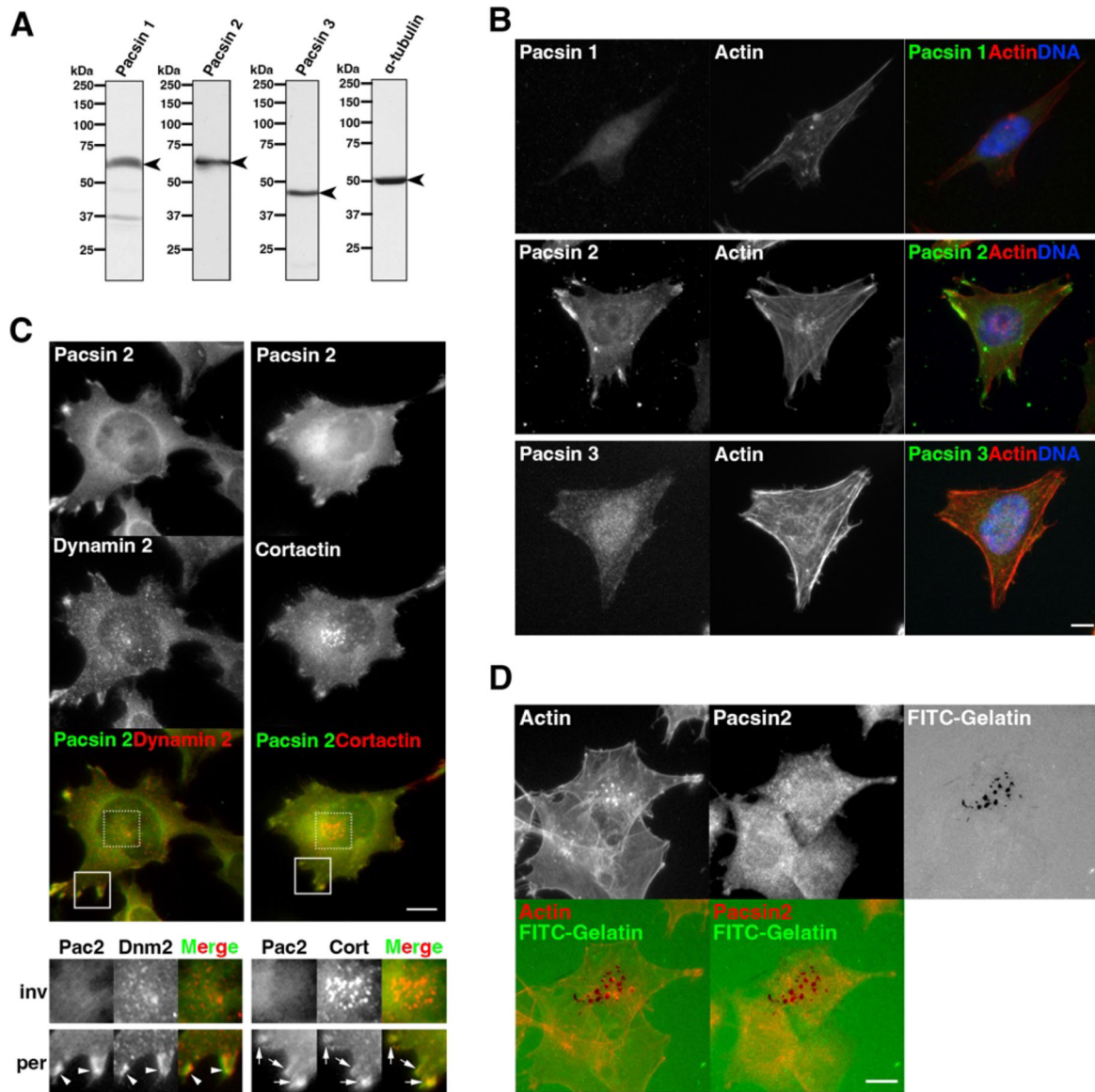


**Fig. 1. Pacsin 2 localises to the cell periphery in T24 cells.** (A) Immunoblot analyses of endogenous pacsin 1, pacsin 2, pacsin 3 and  $\alpha$ -tubulin (arrowheads) in T24 cells. Blots shown are representative of three independent experiments. (B) Localization of endogenous pacsin 1, pacsin 2 and pacsin 3, and of F-actin. Merged images show pacsins (green), F-actin (red) and DNA (blue). (C) Immunofluorescence microscopy images of endogenous pacsin 2 (green) with either endogenous dynamin 2 (red) or endogenous cortactin (red), as indicated. Perinuclear (dashed box) and peripheral (solid box) regions are shown as enlarged images in the lower panel (inv and per, respectively). Colocalization of pacsin 2 (Pac2) with either dynamin 2 (Dnm2, arrowheads) or cortactin (Cort, arrows) in peripheral regions can be observed in the enlarged images. (D) Localization of pacsin 2 (red) or F-actin (red, pseudocolour), as indicated, with FITC-gelatin (green) in T24 cells. Images in B–D are representative of  $n \geq 105$  cells from three independent experiments. Scale bars: 10  $\mu$ m.

T24 cells was analysed by immunofluorescence microscopy. Endogenous N-cadherin colocalized with pacsin 2 and dynamin 2 at the cell periphery in T24 cells (Fig. S2B). Similarly, N-cadherin localized at the cell periphery, as well as in cytoplasmic dots, in control RNAi cells (Fig. 3C, siCtrl). In contrast, in pacsin 2 RNAi cells, N-cadherin accumulated at cell–cell contact sites where actin filaments from contacting cells were interdigitated (Fig. 3C, siPacsin 2 #1, #2 and #3). To probe the relationship between depletion of pacsin 2 and formation of cell–cell contacts more robustly and transparently, we captured low magnification images of the formation of cell–cell contacts by pacsin 2 RNAi cells (Fig. S3). Furthermore, to assess the effects of pacsin 2 depletion on N-cadherin localization at junctions, densely plated control and pacsin 2 RNAi cells were stained for N-cadherin and pacsin 2

(Fig. S4A,B). A similar distribution of N-cadherin to the cell–cell contact sites was also observed in dynamin 2 RNAi cells (Fig. S1C), suggesting a functional association between pacsin 2 and dynamin 2 in the formation of N-cadherin-rich cell–cell contacts.

To determine whether pacsin 2 has conserved roles in the induction of N-cadherin-rich cell junctions, its function was also analysed using the human non-small lung carcinoma cell lines A549 and H1299. Immunoblot analyses showed that H1299 cells, but not A549 cells, have a cadherin expression profile similar to that of T24 cells: N-cadherin expression was detected, but expression of E-, P- and VE-cadherins was not detected (Fig. S5A). Pacsin 2 was also expressed in H1299 cells (Fig. S5B) and colocalized with N-cadherin at the cell periphery (Fig. S5C). As shown in immunoblot analysis, pacsin 2 was efficiently depleted by RNAi in H1299 cells (Fig. S5D). Importantly,

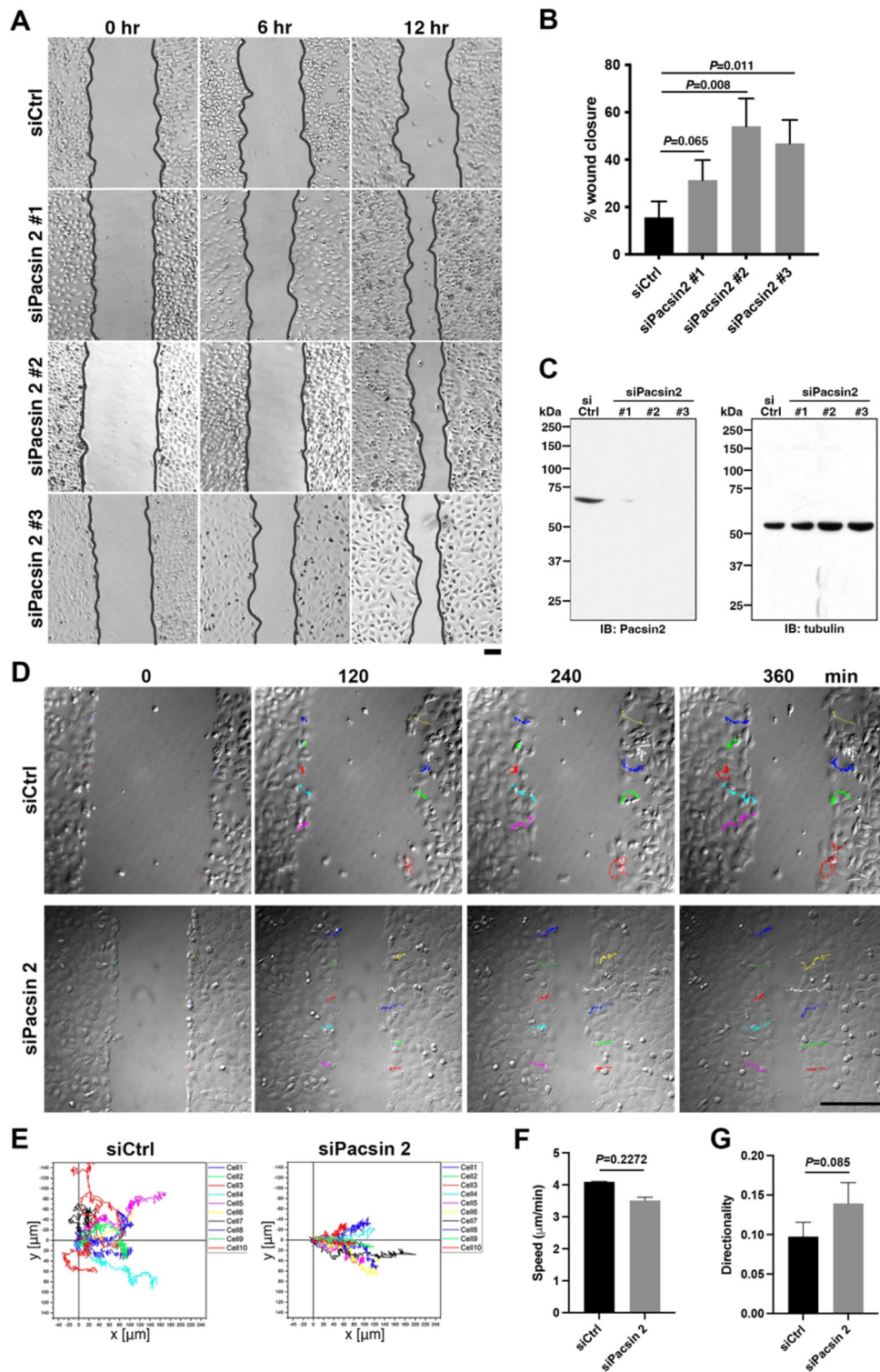


**Fig. 2. Pacsin 2 depletion induces directional cell migration in T24 cells.** (A) Differential interference contrast microscopy images of migrating cells in the wound healing assay. Representative micrographs show either control RNAi cells (siCtrl) or pacsin 2 RNAi cells (siPacsin 2 #1, #2 and #3) at 0, 6 and 12 h after the start of the wound healing assay. Black lines indicate the wound edges. Scale bar: 200 μm. (B) Quantitation of wound closure by either control RNAi cells (siCtrl) or pacsin 2 RNAi cells (siPacsin 2 #1, #2 and #3). Data are mean±s.d. of three independent experiments, five areas each. *P*-values were calculated using an unpaired two-tailed *t*-test. (C) Immunoblot analysis of cell extract from control RNAi cells (siCtrl) and pacsin 2 RNAi cells (siPacsin 2 #1, #2 and #3) using antibodies against pacsin 2 (IB: Pacsin 2) or tubulin as an internal control (IB: tubulin). Blots shown are representative of three independent experiments. (D) Live-cell imaging analysis of the wound healing assay. Time-lapse images of control RNAi (siCtrl) or pacsin 2 RNAi (siPacsin 2) cells at 0, 120, 240 and 360 min after the start of the wound healing assay. Traced paths of ten representative cells are shown in different colours. Scale bar: 100 μm. (E) Trajectories of cell tracking for representative cells over 360 min. The position of each cell at 0 min was set as the origin, and tracks were aligned so that positive *x* displacement values were towards the centre of the wound. (F) Quantitation of cell speed in the wound healing assay. Data are mean±s.d. (*n*=10 cells, *N*=3) in 360 min of the wounding healing assay. (G) Quantitative analysis of cell directionality in the wound healing assay. Data are mean±s.d. (*n*=10 cells, *N*=3) in 360 min of the wounding healing assay. *P*-values in F and G were calculated using an unpaired two-tailed *t*-test.

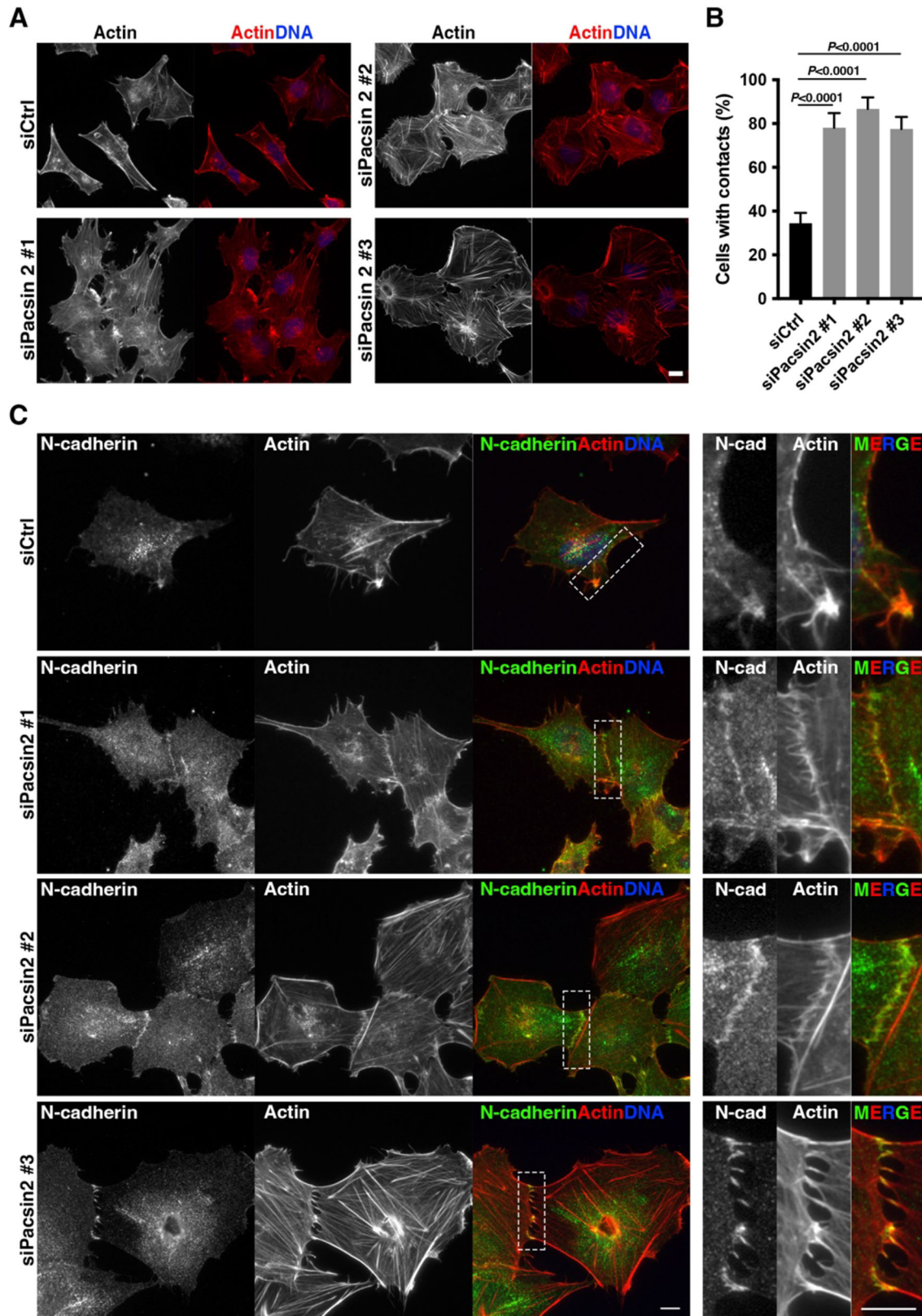


**Fig. 3. Pacsin 2 depletion induces formation of N-cadherin-rich cell–cell contacts in T24 cells.** (A) Immunofluorescence micrographs of control RNAi cells (siCtrl) and pacsin 2 RNAi cells (siPacsin 2 #1, #2 and #3) stained for F-actin. Merged images show F-actin (red) with DNA (blue). Scale bar: 10  $\mu$ m. (B) Quantitation of the percentage of cells with cell contacts in control RNAi cells (siCtrl) and pacsin 2 RNAi cells (siPacsin 2 #1, #2 and #3). Data are mean  $\pm$  s.d. ( $n \geq 120$  cells,  $N=3$ ).  $P$ -values were calculated using an unpaired two-tailed  $t$ -test. (C) Immunofluorescence micrographs of control RNAi cells (siCtrl) and pacsin 2 RNAi cells (siPacsin 2 #1, #2 and #3) stained for endogenous N-cadherin (green), F-actin (red) and DNA (blue). Dashed boxes mark regions of the cell periphery in control cells or N-cadherin-rich cell–cell contact sites in pacsin 2 RNAi cells, and they are shown as enlarged images (right). Images are representative of  $n \geq 150$  cells from three independent experiments. Scale bars: 10  $\mu$ m.

depletion of pacsin 2 in H1299 cells also induced cell–cell contacts enriched with N-cadherin (Fig. S5E,F). To probe the relationship between pacsin 2 depletion and cell–cell contact formation more transparently, we captured low magnification views of the formation of cell–cell contacts by pacsin 2 RNAi cells (Fig. S5G). These results suggest that pacsin 2 has a conserved role in the formation of cell junctions at least within the context of a cancer cell line that expresses only N-cadherin.

To gain further insights into the cell–cell contact sites induced by pacsin 2 RNAi, their ultrastructure was analysed using electron microscopy. Control RNAi cells sometimes formed cell–cell contacts, but structures of the plasma membrane between closely apposed cells were smooth (Fig. 4, siCtrl). In contrast, in pacsin 2 RNAi cells, numerous membranous protrusions were formed at the cell–cell contact sites, and these protrusions were often interdigitating (Fig. 4, siPacsin 2). Immunoblot analyses showed that the total amount of N-cadherin was not altered in pacsin 2 RNAi cells and dynamin 2 RNAi cells (Fig. S6), suggesting that the cell surface level of N-cadherin, but not its transcription and/or translation, is regulated by pacsin 2 and dynamin 2 in T24 cells to induce cell–cell contacts.

#### Depletion of pacsin 2 attenuates N-cadherin endocytosis in T24 cells

The cell surface level of cadherin is determined by a balance between endocytosis, recycling and degradation. Since both pacsin 2 and dynamin 2 have been implicated in endocytosis, we analysed the internalization of surface N-cadherin using a surface biotinylation and endocytosis assay. In both control and pacsin 2 RNAi cells, N-cadherin on the cell surface was internalized within 30 min, and the overall level of internalized N-cadherin then gradually decreased, probably due to degradation (Fig. 5A,B). However, in pacsin 2 RNAi cells, internalization of N-cadherin was attenuated, and the relative amount of internalized N-cadherin was ~46.4% and ~24.2% of that in the control cells at 30 min and 60 min, respectively, after the restart of endocytosis (Fig. 5A,B).

To address whether pacsin 2 plays a direct role in regulating N-cadherin endocytosis, the interaction between pacsin 2 and N-cadherin was examined using a GST pull-down assay. Pacsin 2 contains a C-terminal SH3 domain (Fig. 6A), which binds to proline-rich motifs in its interacting proteins (Dumont and

Lehtonen, 2022). Interestingly, the cytoplasmic domain of N-cadherin contains two PxxP motifs (where x indicates any amino acid), which potentially bind to the SH3 domain of pacsin 2 (Fig. 6A,B). Indeed, endogenous N-cadherin in T24 cells bound to GST-tagged pacsin 2 SH3 domain, but not to GST alone (Fig. 6C). Similarly, both GFP-tagged N-cadherin cytoplasmic domain and GFP-tagged full-length N-cadherin bound to GST-tagged pacsin 2 SH3 domain, but not to GST alone (Fig. 6D,E, Wt). In contrast, the interaction between GST-tagged pacsin 2 SH3 domain and GFP-tagged N-cadherin cytoplasmic domain with proline-to-alanine substitutions in the PxxP motifs was reduced (Fig. 6D, P818/821A and P847/850/851A). Interestingly, the interaction was almost undetectable when GFP-tagged cytoplasmic domain or full-length N-cadherin containing mutations in both PxxP motifs was used in the GST pull-down assay (Fig. 6D,E, P818/821/847/850/851A). These results strongly suggest that pacsin 2 SH3 domain binds to the cytoplasmic domain of N-cadherin via both PxxP motifs to regulate N-cadherin internalization.

We next determined whether expression of the proline-to-alanine mutant form of full-length N-cadherin (P818/821/847/850/851A, referred to hereafter as PA mutant) phenocopies the effects of pacsin 2 depletion. In T24 cells, exogenously expressed GFP-tagged full-length wild-type N-cadherin weakly accumulated at cell–cell contact sites together with another junctional component,  $\alpha$ -catenin (herein referring to  $\alpha$ -catenins in general), where interdigitating F-actin structures were rarely formed (Fig. 6F,G, NCADWt–GFP). In contrast, exogenously expressed GFP-tagged PA mutant N-cadherin localized to the cell–cell contact sites more robustly, together with  $\alpha$ -catenin, often inducing interdigitated F-actin structures (Fig. 6F,G, NCADPA–GFP). Quantitative analyses showed that the signal intensities of GFP-tagged N-cadherin and  $\alpha$ -catenin at cell–cell contact sites were slightly higher in cells expressing PA mutant N-cadherin–GFP than in cells expressing wild-type N-cadherin–GFP, and this difference was found to be statistically significant (Fig. 6H,I). Importantly, the relative intensities of N-cadherin–GFP normalized to  $\alpha$ -catenin were equivalent between wild-type and PA mutants, excluding potential effects of differences in overexpression (Fig. 6J). Consistently, more than 80% of cells formed cell–cell contacts when the N-cadherin PA mutant was expressed, whereas only ~30% of cells showed cell–cell contacts when expressing wild-type

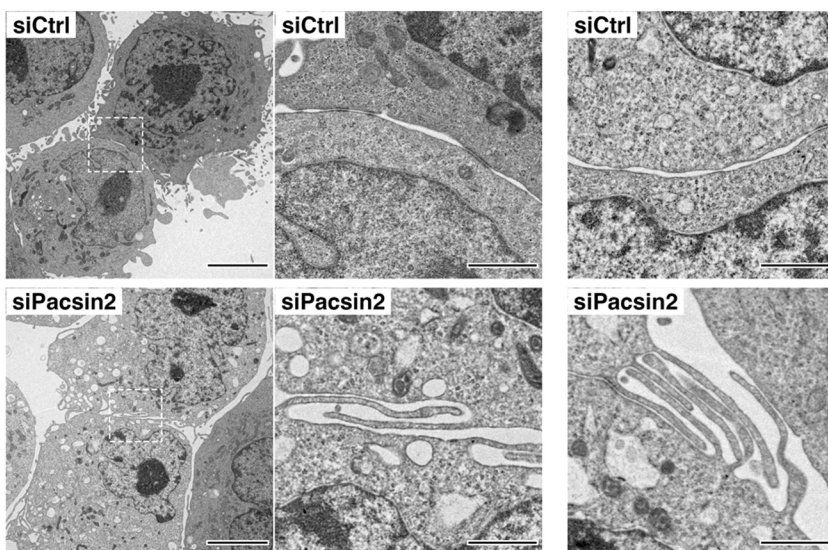


**Fig. 4. Pacsin 2-depleted cells form interdigitating membrane protrusions at cell–cell contact sites in T24 cells.** Transmission electron microscopy images of cell–cell contact sites in control RNAi T24 cells (siCtrl) and pacsin 2 RNAi T24 cells (siPacsin 2) at different magnifications (700 $\times$ , left; 4000 $\times$ , middle and right). Dashed boxes indicate regions shown at higher magnification in the middle panels. Images are representative of  $n \geq 48$  contacts imaged. Scale bars: 5  $\mu$ m (left), 1  $\mu$ m (middle and right).

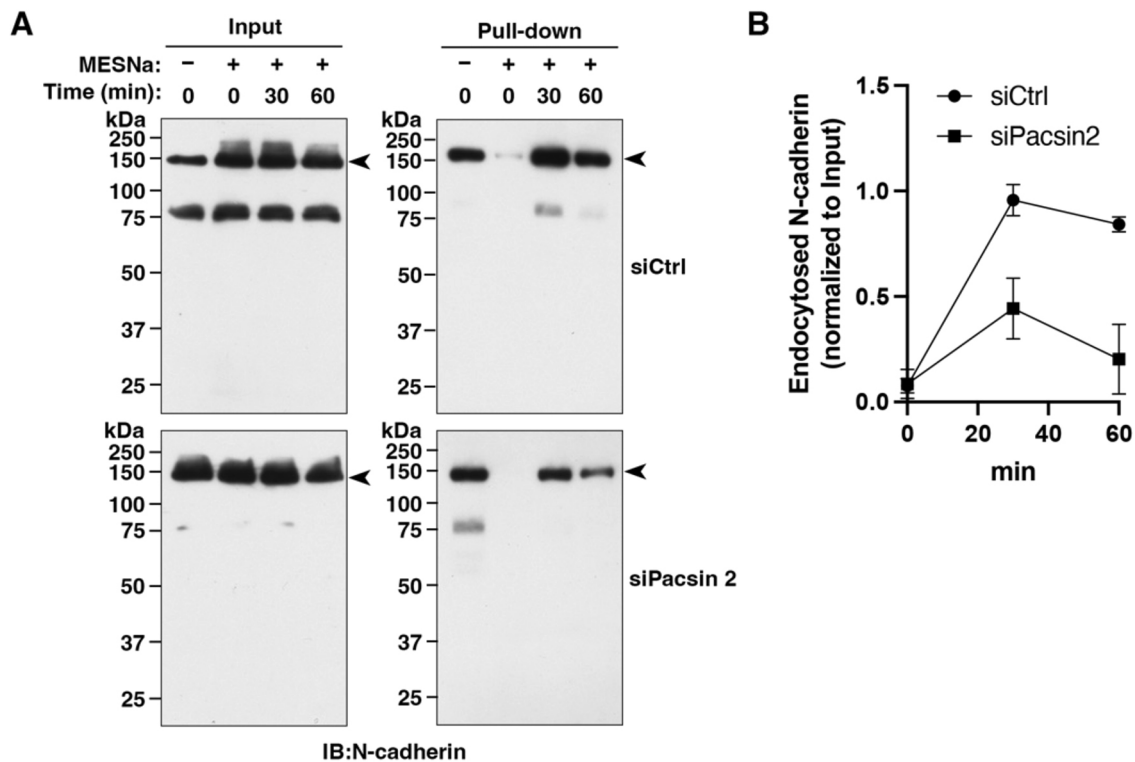


**Fig. 5. Pascin 2 is required for the internalization of N-cadherin.** (A) Representative immunoblots of N-cadherin internalization experiments. Surface N-cadherin in control RNAi T24 cells (siCtrl) and pascin 2 RNAi T24 cells (siPascin 2) was biotinylated at 4°C, and cells were subsequently incubated at 37°C for the indicated periods to allow endocytosis. MESNa was added, as indicated, to remove biotin remaining at the cell surface. Immunoblots (IB) for total N-cadherin (Input, arrowheads) and internalized N-cadherin (Pull-down, arrowheads) are shown. (B) Quantification of internalized N-cadherin in control RNAi cells (siCtrl) and Pascin 2 RNAi cells (siPascin 2) after normalizing the internalized N-cadherin (Pull-down) to the total amount of N-cadherin (Input) in experiments as shown in A. Data are mean±s.d. ( $n=3$ ).

N-cadherin (Fig. 6K). Finally, surface biotinylation and endocytosis assays showed that internalization of the N-cadherin PA mutant was attenuated, and the relative amount of internalized N-cadherin was ~32.5% and ~25.5% of the amount of wild-type N-cadherin at 30 min and 60 min, respectively, after the restart of endocytosis (Fig. 7A,B). These results strongly suggest that pascin 2 interacts with N-cadherin to mediate the N-cadherin internalization required for regulation of collective cell migration of T24 cells.

#### Depletion of pascin 2 and dynamin 2 enhances focal adhesion formation

Collective cell migration requires not only cell–cell adhesion but also integrin-based FAs. A previous study has shown that dynamin 2 is required for the internalization of integrins in NIH-3T3 cells (Ezratty et al., 2005). Consistent with this, dynamin 2 RNAi also induced an increase in the number of FA sites in T24 cells (mean of 19.8 FA sites per cell) compared to the number in control RNAi cells (mean of 3.7 FA sites per cell) (Fig. S7A,B). Similar to the effects of dynamin 2 RNAi, immunofluorescence microscopy showed that the number of paxillin-positive FAs (18.2–29.0 FA sites per cell) exhibited by pascin 2 RNAi cells was more than three times the number observed in control RNAi cells (5.9 FA sites per cell) (Fig. 8A,B). Quantification analyses showed that FAs are preferentially formed in peripheral regions in both pascin 2 RNAi (Fig. 8C) and dynamin 2 RNAi cells (Fig. S7C). Increased FA numbers in pascin 2 RNAi cells and dynamin 2 RNAi cells were also confirmed in single-cell conditions (Fig. S8). These results suggest that pascin 2 and dynamin 2 are involved in the formation of FAs as well as cell–cell contacts that are essential for collective cell migration.

#### DISCUSSION

In this study, we identified pascin 2 as a novel regulator of collective cell migration in various cancer cell lines. Pascin 2-depleted T24 cells migrated in a directional manner (Fig. 2) with an increased number of cell–cell contacts enriched with N-cadherin (Fig. 3). Similarly, pascin 2 depletion also induced N-cadherin-rich cell junctions in the lung cancer cell line H1299 (Fig. S5), suggesting that pascin 2 plays a conserved role as a negative regulator in the formation of N-cadherin-rich cell junctions. In many epithelial cancers, metastasis is facilitated by epithelial-to-mesenchymal transition (EMT) (Nieto et al., 2016). In the EMT, expression profiles of cadherin isoforms are typically switched from E-cadherin to N-cadherin in a process referred to as ‘cadherin switching’, which is associated with increased migratory and invasive behaviour of cancer cells (Wheelock et al., 2008). Previous studies have shown that N-cadherin promotes cell aggregation and collective invasion into collagen matrices, and penetration into mesenchymal layers in lung cancer (Kuriyama et al., 2016) and ovarian cancer (Klymenko et al., 2017). Likewise, in transformed Madin–Darby canine kidney (MDCK) cells, N-cadherin-mediated cell–cell adhesion enhances directional collective cell migration into 3D matrices (Shih and Yamada, 2012). Consistent with this, E-cadherin and N-cadherin were the dominant cadherin isoforms in less aggressive (RT4 and A549) and malignant (T24 and H1299) cancer cells, respectively (Figs S2, S5) (Elie-Caille et al., 2020; Mishra et al., 2018). Cadherin switching is controlled by either transcriptional (Maeda et al., 2005; Thiery and Sleeman, 2006) or post-transcriptional mechanisms (Davis et al., 2003; Ireton et al., 2002; Xiao et al., 2003a). In T24 cells, pascin 2 RNAi and dynamin 2 RNAi both altered the surface

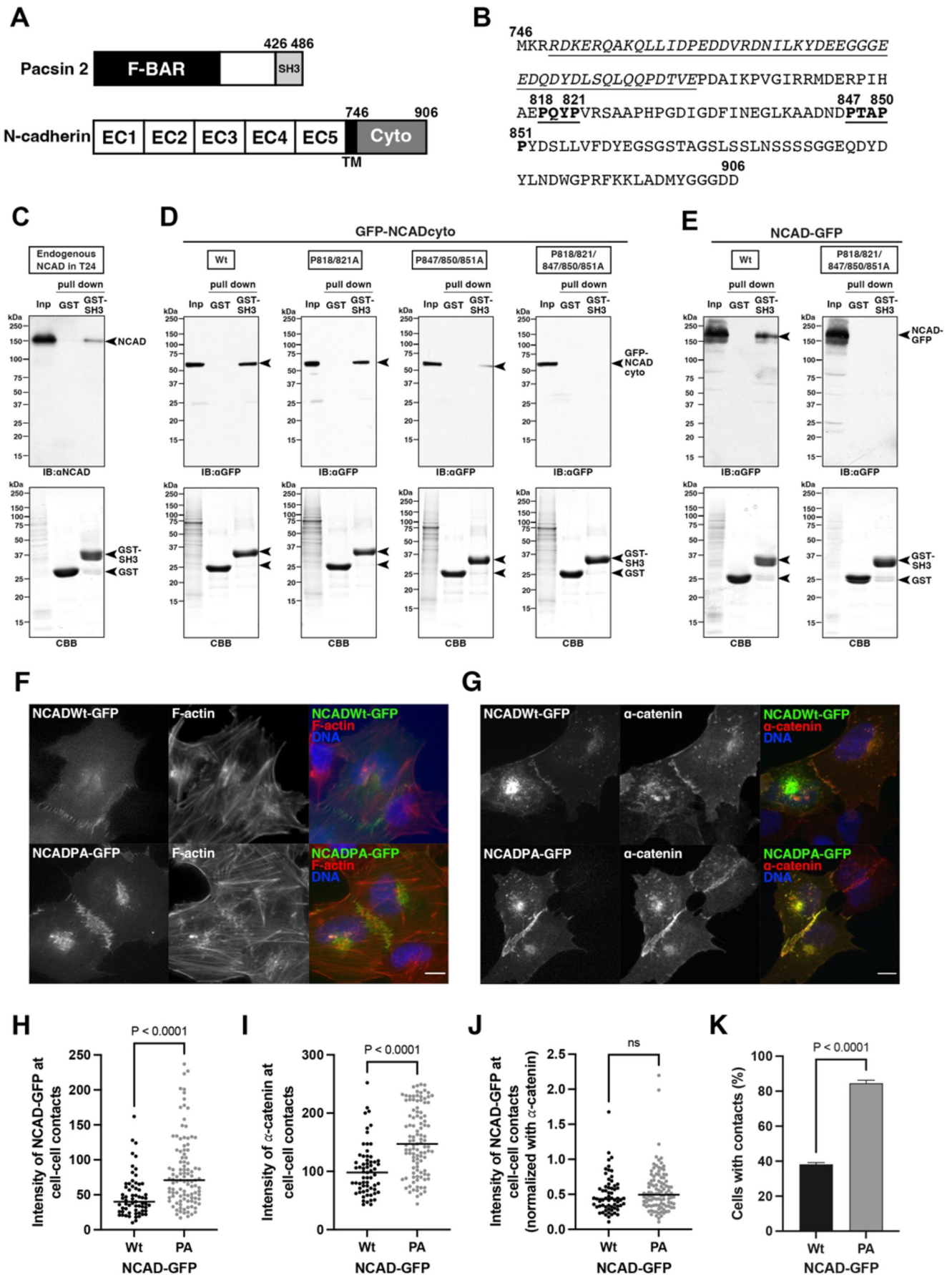


Fig. 6. See next page for legend.



**Fig. 6. Pascin 2 SH3 domain interacts with the N-cadherin cytoplasmic region to regulate cell–cell contact formation.** (A) Schematically illustrated domain structures of human pascin 2 and human N-cadherin. Cyto, cytoplasmic domain; EC, extracellular domain; TM, transmembrane domain. Numbers indicate amino acid positions. (B) Amino acid sequences of the cytoplasmic domain of N-cadherin. Two PxxP motifs (bold and underlined) and p120-binding regions (italicized and underlined) are shown. Numbers indicate amino acid positions. (C) Interaction between pascin 2 SH3 domain and N-cadherin in T24 cells in GST pull-down assays. Immunoblot probed with anti-N-cadherin antibody (IB:  $\alpha$ NCAD) and a CBB-stained SDS–PAGE gel (CBB) for input (Inp; 0.16% of total lysate) and pulled-down fractions with either GST beads (GST) or GST–pascin 2 SH3 beads (GST–SH3) are shown. The positions of endogenous N-cadherin in T24 cells, and of GST–SH3 and GST alone, are marked by arrowheads. (D) Interaction between pascin 2 SH3 domain and N-cadherin cytoplasmic domain in GST pull-down assays. Immunoblots probed with anti-GFP antibody (IB:  $\alpha$ GFP) and CBB-stained SDS–PAGE gels (CBB) for input (Inp; 0.16% of total lysate) and pulled-down fractions with either GST beads (GST) or GST–pascin 2 SH3 beads (GST–SH3) are shown. Positions of wild-type (wt) and mutant (P818/821A, P847/850/851A and P818/821/847/850/851A) forms of GFP-tagged N-cadherin cytoplasmic domain (GFP–NCADcyto), and of GST (GST) and GST-tagged pascin 2 SH3 domain (GST–SH3), are marked by arrowheads. (E) Interaction between pascin 2 SH3 domain and full-length N-cadherin in GST pull-down assays. Immunoblots probed with anti-GFP antibody (IB:  $\alpha$ GFP) and CBB-stained SDS–PAGE gels (CBB) for input (Inp; 0.16% of total lysate) and pulled-down fractions with either GST beads (GST) or GST–pascin 2 SH3 beads (GST–SH3) are shown. Positions of wild-type (Wt) or the PxxP mutant form (P818/821/847/850/851A) of GFP-tagged N-cadherin (NCAD–GFP), and of GST (GST) and GST-tagged pascin 2 SH3 domain (GST–SH3), are marked by arrowheads. Images shown in C–E are representative of three independent experiments. (F) Expression of pascin 2-binding-defective N-cadherin phenocopies the effects of pascin 2 depletion. Immunofluorescence images showing exogenously expressed GFP-tagged wild-type (NCADWt–GFP) or PA mutant (P818/821/847/850/851A) mutations; NCADPA–GFP) N-cadherin, and F-actin in T24 cells. Merged images show GFP-tagged N-cadherin (green), F-actin (red) and DNA (blue). Scale bar: 10  $\mu$ m. (G) Expression of pascin 2-binding-defective N-cadherin induces accumulations of a junctional component. Immunofluorescence images showing exogenously expressed GFP-tagged wild-type (NCADWt–GFP) or PA mutant (NCADPA–GFP) N-cadherin, and  $\alpha$ -catenin in T24 cells. Merged images show GFP-tagged N-cadherin (green),  $\alpha$ -catenin (red) and DNA (blue). Scale bar: 10  $\mu$ m. (H) Quantification of GFP-tagged N-cadherin (NCAD–GFP) signal intensity at cell–cell contact sites for wild-type (Wt) and PA mutant (PA) (Wt,  $n=63$ ; PA,  $n=105$ ). (I) Quantification of  $\alpha$ -catenin signal intensity at cell–cell contact sites in cells expressing either wild-type (Wt) or PA mutant (PA) NCAD–GFP (Wt,  $n=63$ ; PA,  $n=105$ ). (J) The relative intensity of either wild-type (Wt) or PA mutant (PA) NCAD–GFP at cell–cell contact sites, normalized to  $\alpha$ -catenin intensity (Wt,  $n=63$ ; PA,  $n=105$ ). Horizontal lines in H–J indicate the median.  $P$ -values in H–J were calculated using a two-tailed Mann–Whitney test (ns, not significant). (K) Quantification of cell contact formation upon expression of either wild-type (Wt) or PA mutant (PA) NCAD–GFP. Data are presented as mean $\pm$ s.d. ( $n\geq 110$  cells,  $N=3$ ).  $P$ -values were calculated using an unpaired two-tailed  $t$ -test.

level of N-cadherin without affecting its total expression level (Fig. S6), suggesting that pascin 2, as well as dynamin 2, regulates N-cadherin internalization in T24 cells to affect their migratory behaviours.

In this study, we showed that interdigitating membranous protrusions are formed at the N-cadherin-rich cell–cell contact sites in pascin 2 RNAi cells (Fig. 4). In human umbilical vein endothelial cells (HUVECs), VE-cadherin-rich membrane protrusions, known as cadherin fingers or focal adherens junctions (hereafter referred to as FAJs), serve as structural guidance cues that allow coordinated movement of collectively migrating cells (Dorland et al., 2016; Hayer et al., 2016). FAJs are asymmetric junctional structures that extend from the rear of leader cells and are engulfed at the front of follower

cells, exposing topologically opposite membrane curvature to the cytoplasm of the leader cell (negatively curved) and the follower cell (positively curved). The distinct types of membrane curvature in FAJs are capable of selectively recruiting curvature-sensing BAR domain proteins. Indeed, the F-BAR domain protein pascin 2 is recruited to a subset of FAJs, where it plays an important role to maintain cell–cell adhesion (Dorland et al., 2016). Interestingly, our study showed that pascin 2 has the opposite effect on the formation of FAJ-like structures in T24 cells (Figs 3 and 4) and H1299 cells (Fig. S5). However, these results are not mutually exclusive, since multiple BAR domain proteins, such as AMPH1 or nostrin, may contribute to maintaining cell–cell adhesions at FAJs (Dorland et al., 2016; Hayer et al., 2016). Comprehensive analyses of various BAR domain proteins in cell–cell adhesion might reveal their cooperative functions in the formation and/or maintenance of FAJs during collective cell migration.

Pascin 2 colocalized with N-cadherin at the cell periphery in T24 cells (Fig. S2B) and H1299 cells (Fig. S5C). Furthermore, pascin 2 RNAi induced attenuation of N-cadherin internalization in T24 cells (Fig. 5), suggesting that pascin 2 is required for N-cadherin endocytosis. Previous studies have shown that endocytosis of cadherins from the cell surface occurs in either a clathrin-dependent or clathrin-independent manner (Cadwell et al., 2016). In MDCK cells, E-cadherin is constitutively retrieved by clathrin-dependent endocytosis (Le et al., 1999). VE-cadherin in endothelial cells is also endocytosed in a clathrin-dependent manner, resulting in degradation in lysosomes (Xiao et al., 2003b). Similarly, N-cadherin is endocytosed in the clathrin-dependent pathway to facilitate neurite outgrowth (Chen and Tai, 2017). Furthermore, clathrin-dependent endocytosis is also required for the fibroblast growth factor (FGF)-mediated internalization of E-cadherin (Bryant et al., 2005) and vascular endothelial growth factor (VEGF)-mediated internalization of VE-cadherin (Gavard and Gutkind, 2006). A recent study using HUVECs has shown that pascin 2 inhibits VE-cadherin internalization from trailing ends of FAJs without affecting the total surface levels of VE-cadherin (Dorland et al., 2016). However, our study clearly showed that pascin 2 depletion inhibits N-cadherin internalization from the cell surface (Fig. 5). Since the cytoplasmic domains of VE- and N-cadherins are divergent in their amino acid sequences, pascin 2 might associate with multiple cadherins in various ways to control their functions required in specific cell types.

Clathrin-independent endocytic pathways are also involved in the internalization of cadherins, though this process is poorly understood compared to clathrin-dependent endocytosis. Caveolin-dependent endocytosis of E-cadherin is required for disruption of cell–cell adhesion induced by EGF signalling, which is relevant to the EMT of cancer cells (Lu et al., 2003). Another study has shown that Rac1-modulated macropinocytosis is also required for the EGF-induced internalization of E-cadherin in breast carcinoma (Bryant et al., 2007). Clathrin- and caveolae-independent endocytosis is required for N-cadherin internalization to regulate early neuronal maturation *in vivo* (Shikanai et al., 2018). Pascins and dynamins regulate clathrin-dependent endocytosis and caveolae-dependent endocytosis (Dessy et al., 2000; Henley et al., 1998; Qualmann and Kelly, 2000; Senju et al., 2011). Consistently, dynamin 2 RNAi cells phenocopied pascin 2 RNAi cells in the formation of cell–cell contacts enriched with N-cadherin (Fig. S1), suggesting that pascin 2 and dynamin 2 cooperatively regulate the internalization of N-cadherin in clathrin-dependent and/or -independent endocytic pathways.

Clathrin-mediated endocytosis of cadherins is regulated by p120, an armadillo family protein that binds to the cytoplasmic domain of classical cadherin (Reynolds, 2007). In p120-null SW48 colon

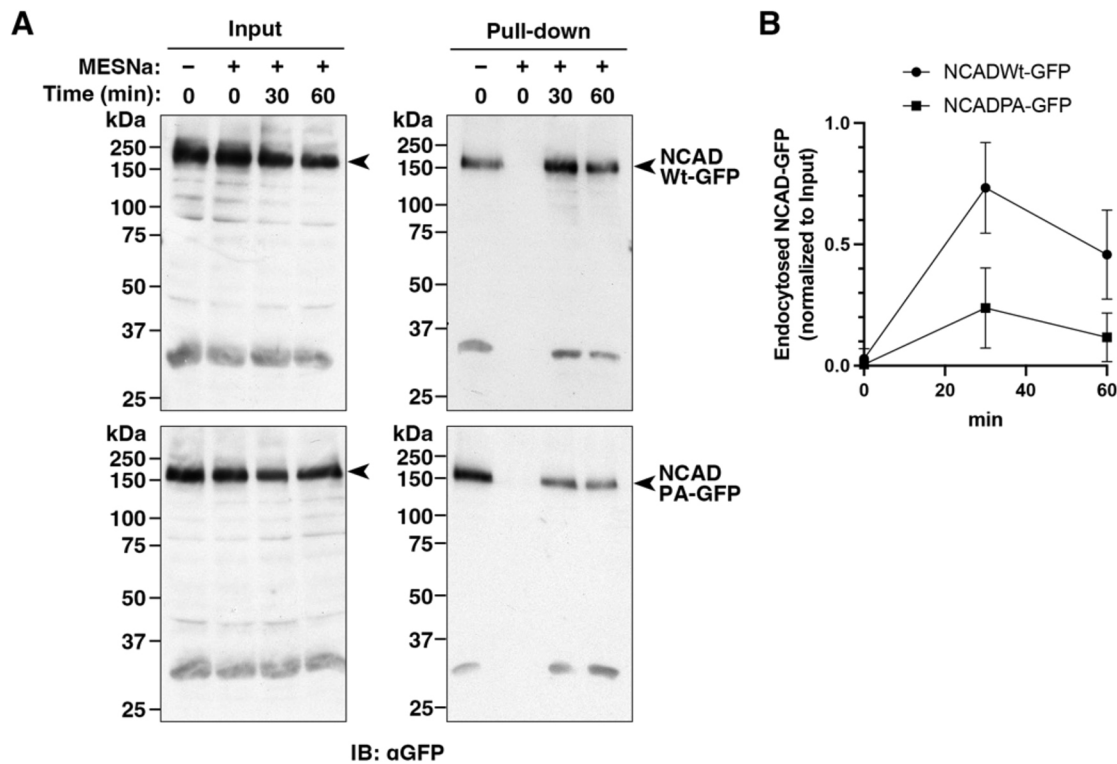


**Fig. 7. A N-cadherin mutant with defective pascins 2 binding shows attenuated internalization.** (A) Representative immunoblots of N-cadherin internalization experiments. Surface GFP-tagged N-cadherin was biotinylated at 4°C, and cells were subsequently incubated at 37°C for the indicated periods to allow endocytosis. MESNa was added, as indicated, to remove biotin remaining at the cell surface. Immunoblots using an anti-GFP antibody (IB:  $\alpha$ GFP) to detect total GFP-tagged N-cadherin (Input, arrowheads) and internalized GFP-tagged N-cadherin (Pull-down, arrowheads) from T24 cells expressing either wild-type (NCADWt-GFP) or PA mutant (NCADPA-GFP) N-cadherin are shown. (B) Quantification of internalized GFP-tagged N-cadherin from cells expressing either wild-type (NCADWt-GFP) or PA mutant (NCADPA-GFP) N-cadherin after normalizing the internalized GFP-tagged N-cadherin (Pull-down) to the total amount of GFP-tagged N-cadherin (Input) in experiments as shown in A. Data are mean $\pm$ s.d. ( $n=3$ ).

carcinoma cells (Ireton et al., 2002) and p120-depleted microvascular endothelial cells (MECs; Xiao et al., 2003a), cadherins are degraded through an endo-lysosomal pathway, revealing that p120 plays essential roles in the regulation of cadherin endocytosis. Interestingly, the pascins 2 SH3 domain bound to cytoplasmic regions of N-cadherin where two PxxP motifs are located in regions distinct from p120-binding sites (Fig. 6B). Indeed, an N-cadherin mutant with proline-to-alanine substitutions in the PxxP motifs failed to bind to pascins 2 SH3 domain (Fig. 6D, E) and induced attenuation of N-cadherin internalization from the cell surface (Fig. 7). Thus, pascins 2 might regulate N-cadherin endocytosis cooperatively with p120 and/or in a novel mechanism independent from p120-mediated regulation of endocytosis.

In this study, we also showed that depletion of either pascins 2 or dynamin 2 increased the number of FAs in T24 cells (Fig. 8; Fig. S7). Increased FA numbers upon pascins 2 RNAi and dynamin 2 RNAi were also observed even in single-cell conditions (Fig. S8), suggesting their direct roles in regulating FA turnover. Indeed, in NIH-3T3 cells, FA disassembly induced by microtubule regrowth after nocodazole washout depends on the recruitment of dynamin 2 to FAs (Ezratty et al., 2005). Another study has shown that the interaction between dynamin 2 and focal adhesion kinase (FAK, also known as PTK2) regulates FA dynamics in response to active Src (Wang et al., 2011). An additional study has shown that the clathrin-dependent pathway is the main pathway for dynamin 2-dependent endocytosis of FA components that leads to FA disassembly (Chao and Kunz, 2009). In contrast to dynamin 2, pascins 2 function in FA turnover is largely unknown. Since pascins 2

and dynamin 2 are cooperatively involved in clathrin-dependent and clathrin-independent endocytosis, further studies are required to reveal their precise function in FA turnover.

In collective cell migration, cell–cell and cell–ECM adhesions need to be finely balanced (Hamidi and Ivaska, 2018). Cell–cell adhesion molecules (e.g. cadherins) and FA molecules (e.g. integrins) share common signalling molecules, and they are physically linked intracellularly via the actin cytoskeleton (Mui et al., 2016). The convergence of crosstalk between these cell adhesion molecules is thought to be Rho-family GTPases (Combedazou et al., 2020). N-cadherin in non-tumour cells enhances collective cell migration via the polarization of Rho-family GTPases essential for cytoskeletal regulation (Mrozik et al., 2018). N-cadherin also facilitates collective cell migration by polarizing FAs in the leading cells by elevating Cdc42 and Rac1 activity towards the free leading edge, resulting in enhanced cell migration (Ouyang et al., 2013; Sabatini et al., 2008; Theveneau et al., 2010). Simultaneously, RhoA is also activated at the lateral and rear sides of the leading cells, inducing enhanced stress fibre formation and actomyosin contractility to establish robust cell–cell contacts (Carmona-Fontaine et al., 2008). The enhanced cell–cell contacts and FAs observed in either pascins 2 RNAi (Figs 3, 8) or dynamin 2 RNAi cells (Figs S1, S7) suggest their key roles in distinct cell adhesion machinery required for coordinated movement of collectively migrating cells.

BAR domain proteins have been implicated in cancer metastasis by controlling cell motility, migration and invasion. CIP4 (Cdc42-interacting protein 4), an F-BAR domain protein, promotes formation

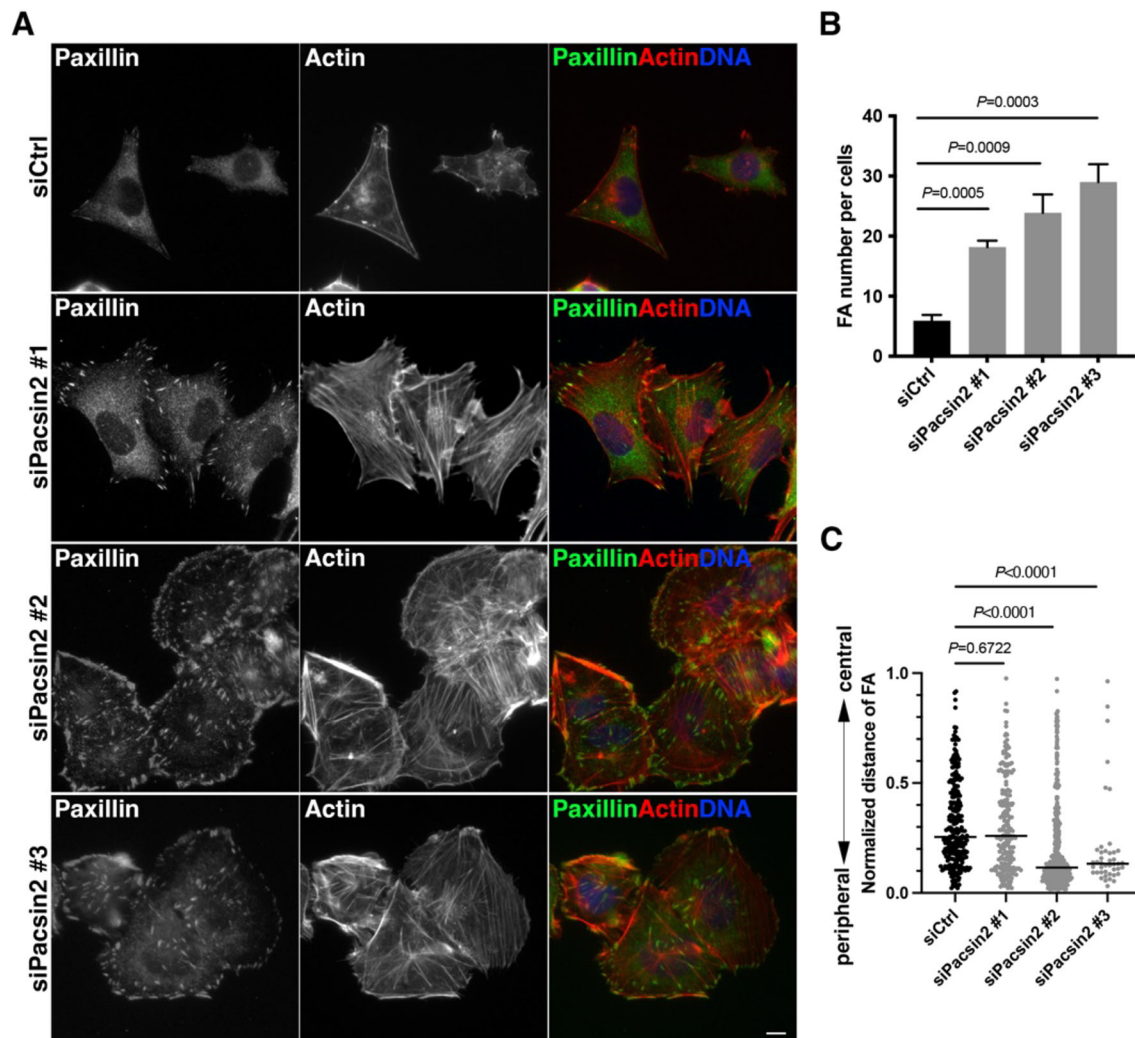


**Fig. 8. Depletion of pacsin 2 induces an elevated number of FAs in T24 cells.** (A) Immunofluorescence micrographs of control RNAi cells (siCtrl) and pacsin 2 RNAi cells (siPacsin 2 #1, #2 and #3) stained for the FA marker paxillin and F-actin. Merged images show paxillin (green), F-actin (red) and DNA (blue). Scale bar: 10  $\mu$ m. (B) Quantitation of FAs per cell in control RNAi cells (siCtrl) and pacsin 2 RNAi cells (siPacsin 2 #1, #2 and #3). Data are means  $\pm$  s.d. ( $n \geq 100$  cells,  $N=3$ ).  $P$ -values were calculated using an unpaired two-tailed  $t$ -test. (C) Spatial distribution of FAs in either control RNAi (siCtrl) or pacsin 2 RNAi (siPacsin 2 #1, #2 and #3) cells. Normalized positions of FAs between the cell periphery (0) and cell centre (1) are shown (control,  $n=272$ ; siPacsin 2 #1,  $n=202$ ; siPacsin 2 #2,  $n=379$ ; siPacsin 2 #3,  $n=43$ ). Horizontal lines mark the median.  $P$ -values were calculated using a two-tailed Mann–Whitney test.

of invadopodia in breast cancer cell lines (Kreider-Letterman et al., 2023; Pichot et al., 2010). Alternative studies using breast cancer cells have shown that CIP4 suppresses Src-induced invadopodia formation by promoting endocytosis of MT1-MMP (also known as MMP14) (Hu et al., 2011). An I-BAR domain protein, MIM (missing in metastasis, also known as MTSS1), suppresses metastasis by regulating cytoskeletal dynamics and lamellipodia formation, consequently affecting the invasion and metastatic behaviour of cancer cells (Woodings et al., 2003). Furthermore, an N-BAR domain protein, endophilin, regulates the endocytosis of EGFR by controlling F-actin cytoskeleton (Vehlow et al., 2013). Interestingly, expression of the brain-specific pacsin isoform pacsin 1 is negatively correlated with the malignancy of gliomas, indicating that pacsin 1 could play an essential role in the development of gliomas and be a potential new biomarker and targeted therapy site for gliomas (Zimu et al., 2021). Collectively migrating cancer cells have higher metastatic potential than singly migrating cells (Yang et al., 2019). Recent findings indicate that collective migration is characteristic of cancer metastasis of epithelial origin (Wang et al., 2016), including ovarian cancer (Choi

et al., 2016), prostate cancer (Cui and Yamada, 2013), breast cancer (Aceto et al., 2014) and colorectal cancer (Chung et al., 2016). Based on TCGA PanCancer Atlas studies in cBioPortal, deep deletions or mutations in the pacsin 2 gene have been identified in samples from people with different types of malignant cancers, including ovarian, breast and bladder cancers (Cerami et al., 2012; Gao et al., 2013). Pacsin 2 has been implicated in various cellular functions such as cell migration (Meng et al., 2011), cell spreading (de Kreuk et al., 2011), EGF receptor internalization (de Kreuk et al., 2012) and collective cell migration (Dorland et al., 2016; Malinova et al., 2021) that are tightly associated with various malignancies. Thus, future studies of the correlation between pacsin 2 expression levels and the malignancy of various cancers might identify pacsin 2 as a potential therapeutic target in cancer metastasis.

## MATERIALS AND METHODS

### Molecular biology

Expression constructs were prepared using Gateway cloning (Thermo Fisher Scientific), as described previously (Fujise et al., 2021). To prepare entry

clones for either full-length N-cadherin and the N-cadherin cytoplasmic domain or the pascin 2 SH3 domain, PCR fragments amplified from clones of human N-cadherin (NM\_001792) or pascin 2 (NM\_001184970) using primers described in Table S1 were used for B–P recombination with either pDONR201 (for full-length N-cadherin and pascin 2 SH3) or pENTR/D-TOPO (for N-cadherin cytoplasmic domain). These entry clones were subcloned into pCI-based destination vectors for expressing GFP-tagged proteins in mammalian cells (N-cadherin cytoplasmic domain and full length) or pGEX6P2 destination vectors for expressing GST-tagged proteins in bacterial cells (pascin 2 SH3) by L–R recombination.

### Cell culture, DNA transfection and RNAi

T24 (ATCC HTB-4), RT4 (ATCC HTB-2), H1299 (ATCC CRL-5803) and A549 (ATCC CCL-185) cells were cultured in RPMI-1640 medium (189-02025, FUJIFILM Wako Chemicals) supplemented with 10% fetal bovine serum (FBS) (26140-079, Gibco) and penicillin-streptomycin (PS) (100 unit/ml) (15140122, Thermo Fisher Scientific) at 37°C in humidified air with 5% CO<sub>2</sub>. HEK293T cells (ATCC CRL-3216) were grown in D-MEM (high glucose) with L-glutamine, Phenol Red, and sodium pyruvate (043-30085, FUJIFILM Wako chemicals) supplemented with 10% FBS (26140-079, Gibco) and PS (100 unit/ml) (15140122, Thermo Fisher Scientific) at 37°C in 5% CO<sub>2</sub>. HUVEC cells (C2519A, Lonza) were cultured on flasks coated with gelatin (G1393, Merck) in EBM-2 Endothelial Cell Basal Medium (CC3156, Lonza) supplemented with EGM-2 Endothelial Cell Growth Medium-2 SingleQuots (CC4176, Lonza) at 37°C in 5% CO<sub>2</sub>.

For transfection of T24 and HEK293T, Lipofectamine LTX with Plus Reagent (15338-100, Thermo Fisher Scientific) was used following the manufacturer's instructions. To transfect T24 cells for immunofluorescence microscopy, 70% confluent cells in VIOLAMO VTC-P24 24-well plates (2-8588-03, AS ONE) were transfected with 0.5 µg of expression plasmids, and cells were fixed 48 h after the transfection. For surface biotinylation and endocytosis assays using T24 cells and GST pull-down assays using HEK293T cells, 70% confluent cells in 100 mm TC-treated culture dishes (430167, Corning) were transfected with 15 µg expression plasmids, and cells were collected 24 h (T24 cells) or 48 h (HEK293T cells) after the transfection to use for further analyses.

For RNAi of T24 cells and H1299 cells, 70% confluent cells in 24-well plates were transfected with 10 pmol of either siGENOME SMART pool siRNA for human Dnm2 (M-04007-03, Dharmacon) or siGENOME nontargeting siRNA Pool #1 (D-001206-13-05, Dharmacon), Mission siRNA for human pascin 2 siRNA [SASI\_Hs01\_0021-5539 (siPascin2#1), SASI\_Hs01\_0021-5540 (siPascin2#2), SASI\_Hs01\_0021-5538 (siPascin2#3); Merck] or MISSION siRNA Universal Negative Control #1 (SIC-001, Merck) using Lipofectamine RNAiMAX Transfection Reagent (13778150, Thermo Fisher Scientific) following manufacturer's instructions. siPascin2#2 (SASI\_Hs01\_0021-5540) was used for figures that just mention siPascin2 (e.g. Fig. 2D–G, Fig. 4, Fig. 5; Movie 2).

### Antibodies and reagents

Primary antibodies used in this study were rabbit polyclonal anti-dynamin 2 (ab65556, Abcam), rabbit polyclonal anti-PACIN1 (M-46; sc-30127, Santa Cruz Biotechnology), mouse monoclonal anti-PACIN 2 (SAB1402538-100UG, SIGMA), mouse monoclonal anti-PACIN3 (C-3; sc-166923, Santa Cruz Biotechnology), mouse monoclonal anti-E-cadherin (610181, BD Transduction laboratory), mouse monoclonal anti-N-cadherin (610920, BD Transduction laboratory), mouse monoclonal anti-P-cadherin (12H6, Cell Signaling Technology), mouse monoclonal anti-VE-cadherin (610251, BD Transduction laboratory), mouse monoclonal anti-paxillin (5H11) (AH00492, Thermo Fisher Scientific), mouse monoclonal anti- $\alpha$ -tubulin (T5168, Merck), rabbit polyclonal anti-cortactin (A302-608A-M, Thermo Fisher Scientific), anti-GFP (D5.1) XP rabbit mAb (2956, Cell Signaling Technology) and mouse monoclonal  $\alpha$ -catenin (G-11) (sc-9988, Santa Cruz Biotechnology). Secondary antibodies and Alexa Fluor-conjugated phalloidin for immunofluorescence microscopy were purchased from Thermo Fisher Scientific: Alexa Fluor 488 donkey anti-goat IgG (H+L) (A-11055), Alexa Fluor 488 donkey anti-rabbit IgG (H+L)

(A-21206), Alexa Fluor 555 donkey anti-mouse IgG (H+L) (A-31570), Alexa Fluor 555 donkey anti-rabbit IgG (H+L) (A-31572) and Alexa Fluor 555 Phalloidin (A-34055). Secondary antibodies for immunoblot analyses were also purchased from Thermo Fisher Scientific: goat anti-rabbit IgG (H+L) secondary antibody, HRP (31460); and rabbit anti-mouse IgG (H+L) secondary antibody, HRP (31450).

Paraformaldehyde used for cell fixation was prepared from 16% paraformaldehyde (15710, Electron Microscopy Sciences). Glutaraldehyde used for fixing gelatin-coated coverslips was prepared from glutaraldehyde 25% EM (G004, TAAB).

### Immunofluorescence microscopy

Immunofluorescence microscopy of T24 and H1299 cells on gelatin-coated coverslips was performed as described previously (Li et al., 2021) using primary antibodies (1:100 dilution for anti-N-cadherin; 1:200 dilution for anti-dynamin 2, anti-cortactin, anti-paxillin and anti-pascin 2; 1:500 dilution for anti-pascin 1 and anti-pascin 3; and 1:400 for anti- $\alpha$ -catenin) and secondary antibodies (1:1000 dilution), as well as Alexa Fluor 555 Phalloidin (1:1000 dilution). DNA was stained using 1:10,000 dilution of Hoechst 33258 (343-07961, DOJINDO). FITC–gelatin was also prepared as described previously (Li et al., 2021). Immunostained samples for T24 cells were visualized using a BX51 fluorescence microscope (OLYMPUS) with a 40× NA 0.75 objective lens, and images were acquired with Discovery MH15 CMOS camera (Tucson) and ISCcapture image acquisition software (Tucson). All images were analysed using Fiji (Schindelin et al., 2012) and processed with Adobe Photoshop 2022 (Adobe).

### Immunoblot analysis

Immunoblot analyses were performed as described previously (Fujise et al., 2021) using primary antibodies (1:1000 dilution) and secondary antibodies (1:10,000 dilution). For signal detection, either Amersham ECL Prime (RPN2232, Cytiva) or SuperSignal West Pico PLUS Chemiluminescent Substrate (34580, Thermo Fisher Scientific) was used. For Coomassie Brilliant Blue (CBB) staining, Brilliant Blue R (27816, Merck) was used at 0.225% (w/v) in 50% (v/v) methanol and 10% (v/v) acetic acid.

### Wound healing assay

Confluent T24 cells transfected with siRNAs for control and pascin 2 RNAi in 6-well plates were treated with 10 ng/ml of recombinant human EGF (236-EG, R&D systems) in RPMI-1640 medium and incubated at 37°C, 5% CO<sub>2</sub> for 2 h. After 2 h, the cell monolayer was scratched with a sterile 200 µl pipette tip. Recovery processes were captured after 0, 6 and 12 h using a NEX-5N camera (Sony) attached to a Nikon Eclipse Ts2 microscope using a 2× objective lens.

For live-cell imaging of the wound healing assay, T24 cells ( $0.6 \times 10^6$  cells) transfected with either control siRNA or pascin 2 siRNA were seeded in a 35 mm glass-base dish (3910-035, IWAKI) and incubated at 37°C, 5% CO<sub>2</sub> until the cell monolayer became confluent. Cells were then treated with 10 ng/ml of recombinant human EGF (236-EG, R&D systems) in RPMI-1640 medium and incubated at 37°C, 5% CO<sub>2</sub> for 2 h. After the cell monolayer was scratched with a sterile 20 µl pipette tip, cells were maintained in 5% CO<sub>2</sub> at 37°C with a thermo-control system (MI-IBC, OLYMPUS), and images were acquired on an IX71 microscope (OLYMPUS) fitted with an X-Light spinning disc confocal unit (CrestOptics) and iXon EMCCD camera (DU-888E-C00-#BV, ANDOR) using MetaMorph (Molecular Devices). Images were captured with a 20× objective lens (LCPlanFI 20×/0.40) at 1-min intervals for 6 h.

For cell tracking analyses, ten cells at the front of either side of the wound edge were randomly selected and tracked using the Manual Tracking plugins of Fiji (Schindelin et al., 2012). Cell velocity and directionality were determined by analysing the trajectories of 10 cells/movie from four independent movies (40 cells each for control and pascin 2 RNAi) using the Chemotaxis Tool (ibidi). Cell traces were analysed using OriginPro 2021 (Origin Lab).

### GST pull-down assays

The recombinant protein of human pascin 2 SH3 domain (amino acids 426–486) used as bait for the GST pull-down assay was expressed and

purified with the GST Gene Fusion System (Cytiva) as a GST fusion using Glutathione Sepharose 4B (17075601, Cytiva) according to the manufacturer's instructions. The GFP-tagged cytoplasmic domain of N-cadherin (amino acids 746–906) was expressed in HEK293T cells, and the cell extract was prepared by sonication using a TAITEC VP-5S sonicator (output: 5; 3×5 s) in extraction buffer [20 mM Tris-HCl, pH 7.5, 150 mM NaCl, 10% glycerol, 5 mM EDTA, 2% Triton X-100, 1 mM PMSF and protease inhibitor (11697498001, Roche)] followed by centrifugation at 20,600 *g* for 10 min at 4°C. For the pull-down assay, 170 µl of the cell extract was added to 10 µl (bed volume) of GST–pascin 2 SH3 or GST beads in the extraction buffer and mixed for 1 h at 4°C with gentle agitation. After washing three times with the extraction buffer, the bound proteins were analysed by immunoblot analyses.

### Surface biotinylation and endocytosis assay

The surface biotinylation and endocytosis assay was performed as described previously (Morimoto et al., 2005) with minor modifications. T24 cells ( $2.5 \times 10^5$  cells) transfected with control siRNA or pascin 2 siRNA for 48 h were seeded in a 100 mm TC-treated culture dish (430167, Corning) in RPMI-1640 medium. Alternatively, T24 cells ( $3.2 \times 10^6$  cells) in a 100 mm TC-treated culture dish were transfected with constructs encoding either GFP-tagged full-length wild-type N-cadherin (NCADWt–GFP) or GFP-tagged full-length PA mutant N-cadherin (NCADPA–GFP). After 24 h, cell surface proteins were biotinylated with 0.5 mg/ml Ez-link sulfo-NHS-SS-Biotin (21331, Thermo Fisher Scientific) in PBS containing 1 mM CaCl<sub>2</sub> and 0.5 mM MgCl<sub>2</sub> (PBS/CM) at 4°C for 30 min, and quenched with 50 mM NH<sub>4</sub>Cl in PBS/CM at 4°C for 15 min. The cells were then allowed to endocytose at 37°C for the indicated periods until the endocytosis was stopped by rapid cooling of the cells on ice at 4°C. The remaining biotin on the cell surface was stripped with 50 mM sodium 2-mercaptoethanesulfonate (MESNa) (M1511, Sigma-Aldrich) in PBS/CM at 4°C for 30 min followed by quenching with 5 mg/ml iodoacetamide (093-02152, Fujifilm) in PBS/CM at 4°C for 15 min. Cells were then lysed with RIPA buffer [20 mM Tris-HCl pH 7.6, 150 mM NaCl, 0.1% SDS, 1% Triton X-100, 1% deoxycholate, 5 mM EDTA with protease inhibitors (11697498001, Roche)] by sonication using a TAITEC VP-5S sonicator (output: 5; 2×5 s), and cell lysate was recovered in the supernatant after centrifugation at 20,000 *g* at 4°C for 15 min. The cell lysates containing an equal amount of total proteins ( $\approx 2$  mg in 1 ml RIPA buffer) were incubated with 15 µl (bed volume) of Pierce NeutrAvidin agarose (29200, Thermo Fisher Scientific) for 2 h at 4°C to capture internalized biotinylated protein. After washing three times in RIPA buffer, biotinylated proteins were eluted from NeutrAvidin agarose beads by sample buffer, separated by SDS–PAGE and analysed by immunoblotting using an antibody against N-cadherin. The relative amount of internalized N-cadherin (pull-down) was obtained by normalizing it to the total amount of N-cadherin expressed in the cells.

### Electron microscopy

T24 cells were fixed in 2% glutaraldehyde and 2% paraformaldehyde at 4°C overnight and then post fixed in 2% osmium tetroxide for 1.5 h at 4°C followed by dehydration with ethanol and embedding in Spurr resin (Polysciences Inc., Warrington, PA, USA). Ultrathin sections of the samples were prepared using an ultramicrotome (Leica EM UC7), and they were stained with uranyl acetate and lead and observed by electron microscope H-7650 (Hitachi, Tokyo, Japan) at Central Research Laboratory (Okayama University Medical School).

### Image analyses of N-cadherin and FAs

To quantitatively evaluate the localization of GFP-tagged N-cadherin or  $\alpha$ -catenin, 25×25-pixel regions of interest (ROIs) were manually located on cell–cell contact sites, and then maximum intensities were measured from the 2-pixel-Gaussian filtered fluorescently labelled N-cadherin images using ImageJ software (Schneider et al., 2012). Intensity ratios of GFP-tagged N-cadherin to  $\alpha$ -catenin were also calculated.

To quantitatively evaluate the intracellular distribution of FAs, automatic image processing was performed using ImageJ. First, the cell regions were

determined by the Triangle intensity thresholding of 5–35-pixel-band-pass filtered images of fluorescently labelled actin filaments. Next, using the 'Distance Map' function in ImageJ, the relative position from the cell contour was quantified. The position of the cell contour was given a minimum value of 0 and the position farthest from the cell contour was given a maximum value of 1. Then, the regions of FAs in the cell regions were automatically detected by the Yen's intensity thresholding of 1–4-pixel-band-pass filtered images of fluorescently labelled paxillin. Finally, the average distance from the cell periphery of FA regions with more than 30 pixels was measured.

### Statistical analysis

All the experiments were repeated three times independently. Data were analysed for statistical significance using GraphPad Prism6 (GraphPad Software).

### Acknowledgements

The authors thank Ms Masumi Furutani and Ms Moemi Tsukano (Central Research Laboratory, Okayama University Medical School) for their technical assistance in sample preparation and observation of electron microscopy. The authors also thank Dr Harvey McMahon (MRC-LMB, UK) for reagents.

### Competing interests

The authors declare no competing or financial interests.

### Author contributions

Conceptualization: Y.N., M.W., T.T.; Methodology: T.T.; Software: T.T.; Validation: T.H., K.T., T.T.; Formal analysis: H.W., J.L., T.H., T.T.; Investigation: H.W., J.L., T.T.; Resources: T.T.; Data curation: H.W., J.L., T.A., H.Y., T.T.; Writing - original draft: H.W., T.H., T.T.; Writing - review & editing: H.W., J.L., T.A., H.Y., Y.N., M.W., K.T., T.T.; Visualization: T.H., T.T.; Supervision: K.T., T.T.; Project administration: K.T., T.T.; Funding acquisition: T.H., M.W., K.T., T.T.

### Funding

This work was supported by Japan Society for the Promotion of Science KAKENHI grant numbers 18K07198 and 19KK0180 to T.T., 19H03225 to K.T., and 19H01064 to M.W., as well as grants from Wesco Science Foundation to T.T. This work was also supported by Japan Society for the Promotion of Science KAKENHI grant number JP22H04926. Grant-in-Aid for Transformative Research Areas –Platforms for Advanced Technologies and Research Resources 'Advanced Bioimaging Support'. Open access funding provided by Okayama University. Deposited in PMC for immediate release.

### Data availability

All relevant data can be found within the article and its supplementary information.

### First Person

This article has an associated First Person interview with the first author of the paper.

### Peer review history

The peer review history is available online at <https://journals.biologists.com/jcs/lookup/doi/10.1242/jcs.260827.reviewer-comments.pdf>.

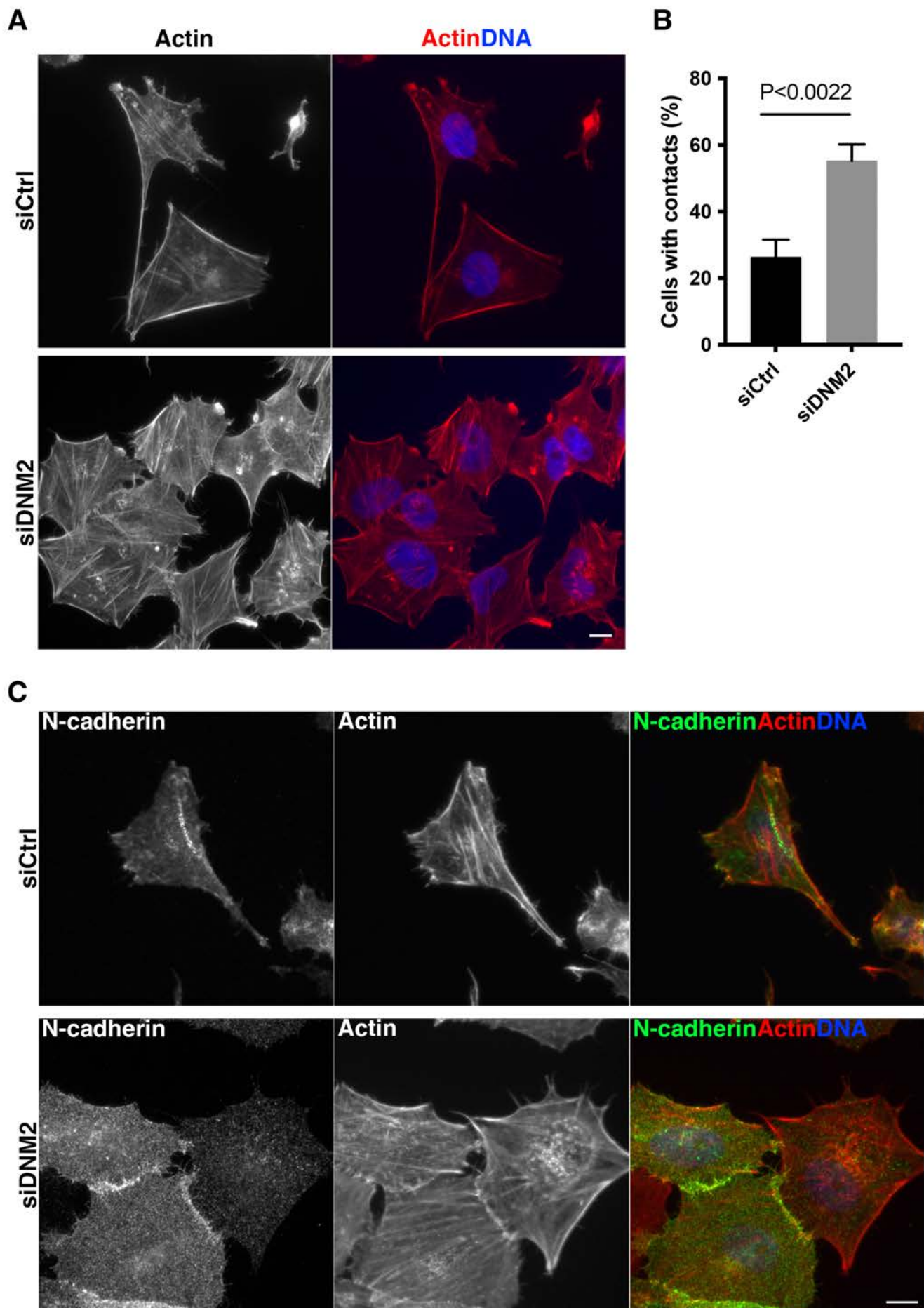
### References

- Aceto, N., Bardia, A., Miyamoto, D. T., Donaldson, M. C., Wittner, B. S., Spencer, J. A., Yu, M., Pely, A., Engstrom, A., Zhu, H. et al. (2014). Circulating tumor cell clusters are oligoclonal precursors of breast cancer metastasis. *Cell* **158**, 1110–1122. doi:10.1016/j.cell.2014.07.013
- Akhtar, N. and Hotchin, N. A. (2001). Rac1 regulates adherens junctions through endocytosis of E-cadherin. *Mol. Biol. Cell* **12**, 847–862. doi:10.1091/mbc.12.4.847
- Bryant, D. M., Wylie, F. G. and Stow, J. L. (2005). Regulation of endocytosis, nuclear translocation, and signaling of fibroblast growth factor receptor 1 by E-cadherin. *Mol. Biol. Cell* **16**, 14–23. doi:10.1091/mbc.e04-09-0845
- Bryant, D. M., Kerr, M. C., Hammond, L. A., Joseph, S. R., Mostov, K. E., Teasdale, R. D. and Stow, J. L. (2007). EGF induces macropinocytosis and SNX1-modulated recycling of E-cadherin. *J. Cell Sci.* **120**, 1818–1828. doi:10.1242/jcs.000653
- Cadwell, C. M., Su, W. and Kowalczyk, A. P. (2016). Cadherin tales: regulation of cadherin function by endocytic membrane trafficking. *Traffic* **17**, 1262–1271. doi:10.1111/tra.12448
- Carmona-Fontaine, C., Matthews, H. K., Kuriyama, S., Moreno, M., Dunn, G. A., Parsons, M., Stern, C. D. and Mayor, R. (2008). Contact inhibition of locomotion

- in vivo controls neural crest directional migration. *Nature* **456**, 957-961. doi:10.1038/nature07441
- Cerami, E., Gao, J., Dogrusoz, U., Gross, B. E., Sumer, S. O., Aksoy, B. A., Jacobsen, A., Byrne, C. J., Heuer, M. L., Larsson, E. et al.** (2012). The cBio cancer genomics portal: an open platform for exploring multidimensional cancer genomics data. *Cancer Discov.* **2**, 401-404. doi:10.1158/2159-8290.CD-12-0095
- Chandrasekaran, R., Kenworthy, A. K. and Lacy, D. B.** (2016). Clostridium difficile Toxin A undergoes clathrin-independent, PACSIN2-dependent endocytosis. *PLoS Pathog.* **12**, 1-30. doi:10.1371/journal.ppat.1006070
- Chao, W.-T. and Kunz, J.** (2009). Focal adhesion disassembly requires clathrin-dependent endocytosis of integrins. *FEBS Lett.* **583**, 1337-1343. doi:10.1016/j.febslet.2009.03.037
- Chen, Y.-T. and Tai, C.-Y.** (2017).  $\mu$ 2-Dependent endocytosis of N-cadherin is regulated by  $\beta$ -catenin to facilitate neurite outgrowth. *Traffic* **18**, 287-303. doi:10.1111/tra.12473
- Chiasson, C. M., Wittich, K. B., Vincent, P. A., Faundez, V. and Kowalczyk, A. P.** (2009). p120-catenin inhibits VE-cadherin internalization through a Rho-independent mechanism. *Mol. Biol. Cell* **20**, 1970-1980. doi:10.1091/mbc.e08-07-0735
- Choi, P.-W., Yang, J., Ng, S.-K., Feltmate, C., Muto, M. G., Hasselblatt, K., Lafferty-Whyte, K., JeBailey, L., MacConaill, L., Welch, W. R. et al.** (2016). Loss of E-cadherin disrupts ovarian epithelial inclusion cyst formation and collective cell movement in ovarian cancer cells. *Oncotarget* **7**, 4110-4121. doi:10.18632/oncotarget.6588
- Chung, Y.-C., Wei, W.-C., Hung, C.-N., Kuo, J.-F., Hsu, C.-P., Chang, K.-J. and Chao, W.-T.** (2016). Rab11 collaborates E-cadherin to promote collective cell migration and indicates a poor prognosis in colorectal carcinoma. *Eur. J. Clin. Invest.* **46**, 1002-1011. doi:10.1111/eci.12683
- Combedazou, A., Gayral, S., Colombié, N., Fougere, A., Laffargue, M. and Ramel, D.** (2020). Small GTPases orchestrate cell-cell communication during collective cell movement. *Small GTPases* **11**, 103-112. doi:10.1080/21541248.2017.1366965
- Cui, Y. and Yamada, S.** (2013). N-cadherin dependent collective cell invasion of prostate cancer cells is regulated by the N-terminus of alpha-catenin. *PLoS ONE* **8**, e55069. doi:10.1371/journal.pone.0055069
- Davis, M. A., Ireton, R. C. and Reynolds, A. B.** (2003). A core function for p120-catenin in cadherin turnover. *J. Cell Biol.* **163**, 525-534. doi:10.1083/jcb.200307111
- de Kreuk, B.-J., Nethe, M., Fernandez-Borja, M., Anthony, E. C., Hensbergen, P. J., Deelder, A. M., Plomann, M. and Hordijk, P. L.** (2011). The F-BAR domain protein PACSIN2 associates with Rac1 and regulates cell spreading and migration. *J. Cell Sci.* **124**, 2375-2388. doi:10.1242/jcs.080630
- de Kreuk, B.-J., Anthony, E. C., Geerts, D. and Hordijk, P. L.** (2012). The F-BAR protein PACSIN2 regulates epidermal growth factor receptor internalization. *J. Biol. Chem.* **287**, 43438-43453. doi:10.1074/jbc.M112.391078
- Dessy, C., Kelly, R. A., Balligand, J. L. and Feron, O.** (2000). Dynamin mediates caveolar sequestration of muscarinic cholinergic receptors and alteration in NO signaling. *EMBO J.* **19**, 4272-4280. doi:10.1093/emboj/19.16.4272
- Dorland, Y. L., Malinova, T. S., van Stalborch, A.-M. D., Grieve, A. G., van Geemen, D., Jansen, N. S., de Kreuk, B.-J., Nawaz, K., Kole, J., Geerts, D. et al.** (2016). The F-BAR protein pacsin2 inhibits asymmetric VE-cadherin internalization from tensile adherens junctions. *Nat. Commun.* **7**, 12210. doi:10.1038/ncomms12210
- Dumont, V. and Lehtonen, S.** (2022). PACSIN proteins in vivo: roles in development and physiology. *Acta Physiol. (Oxf.)* **234**, e13783. doi:10.1111/apha.13783
- Elie-Caille, C., Lascombe, I., Péchery, A., Bittard, H. and Fauconnet, S.** (2020). Molecular and nanoscale evaluation of N-cadherin expression in invasive bladder cancer cells under control conditions or GW501516 exposure. *Mol. Cell. Biochem.* **471**, 113-127. doi:10.1007/s11010-020-03771-1
- Ezratty, E. J., Partridge, M. A. and Gundersen, G. G.** (2005). Microtubule-induced focal adhesion disassembly is mediated by dynamin and focal adhesion kinase. *Nat. Cell Biol.* **7**, 581-590. doi:10.1038/ncb1262
- Friedl, P. and Gilmour, D.** (2009). Collective cell migration in morphogenesis, regeneration and cancer. *Nat. Rev. Mol. Cell Biol.* **10**, 445-457. doi:10.1038/nrm2720
- Fujise, K., Okubo, M., Abe, T., Yamada, H., Nishino, I., Noguchi, S., Takei, K. and Takeda, T.** (2021). Mutant BIN1-Dynamin 2 complexes dysregulate membrane remodeling in the pathogenesis of centronuclear myopathy. *J. Biol. Chem.* **296**, 100077. doi:10.1074/jbc.RA120.015184
- Gao, J., Aksoy, B. A., Dogrusoz, U., Dresdner, G., Gross, B., Sumer, S. O., Sun, Y., Jacobsen, A., Sinha, R., Larsson, E. et al.** (2013). Integrative analysis of complex cancer genomics and clinical profiles using the cBioPortal. *Sci. Signal.* **6**, pii. doi:10.1126/scisignal.2004088
- Gavard, J. and Gutkind, J. S.** (2006). VEGF controls endothelial-cell permeability by promoting the  $\beta$ -arrestin-dependent endocytosis of VE-cadherin. *Nat. Cell Biol.* **8**, 1223-1234. doi:10.1038/ncb1486
- Gumbiner, B. M.** (2005). Regulation of cadherin-mediated adhesion in morphogenesis. *Nat. Rev. Mol. Cell Biol.* **6**, 622-634. doi:10.1038/nrm1699
- Haeger, A., Wolf, K., Zegers, M. M. and Friedl, P.** (2015). Collective cell migration: Guidance principles and hierarchies. *Trends Cell Biol.* **25**, 556-566. doi:10.1016/j.tcb.2015.06.003
- Hallbleib, J. M. and Nelson, W. J.** (2006). Cadherins in development: cell adhesion, sorting, and tissue morphogenesis. *Genes Dev.* **20**, 3199-3214. doi:10.1101/gad.1486806
- Hamidi, H. and Ivaska, J.** (2018). Every step of the way: integrins in cancer progression and metastasis. *Nat. Rev. Cancer* **18**, 533-548. doi:10.1038/s41568-018-0038-z
- Hansen, C. G., Howard, G. and Nichols, B. J.** (2011). Pacsin 2 is recruited to caveolae and functions in caveolar biogenesis. *J. Cell Sci.* **124**, 2777-2785. doi:10.1242/jcs.084319
- Hayer, A., Shao, L., Chung, M., Joubert, L.-M., Yang, H. W., Tsai, F.-C., Bisaria, A., Betzig, E. and Meyer, T.** (2016). Engulfed cadherin fingers are polarized junctional structures between collectively migrating endothelial cells. *Nat. Cell Biol.* **18**, 1311-1323. doi:10.1038/ncb3438
- Henley, J. R., Krueger, E. W. A., Oswald, B. J. and McNiven, M. A.** (1998). Dynamin-mediated internalization of caveolae. *J. Cell Biol.* **141**, 85-99. doi:10.1083/jcb.141.1.85
- Hu, J., Mukhopadhyay, A., Truesdell, P., Chander, H., Mukhopadhyay, U. K., Mak, A. S. and Craig, A. W. B.** (2011). Cdc42-interacting protein 4 is a Src substrate that regulates invadopodia and invasiveness of breast tumors by promoting MT1-MMP endocytosis. *J. Cell Sci.* **124**, 1739-1751. doi:10.1242/jcs.078014
- Ireton, R. C., Davis, M. A., van Hengel, J., Mariner, D. J., Barnes, K., Thoreson, M. A., Anastasiadis, P. Z., Matrisian, L., Bundy, L. M., Sealy, L. et al.** (2002). A novel role for p120 catenin in E-cadherin function. *J. Cell Biol.* **159**, 465-476. doi:10.1083/jcb.200205115
- Kaszak, I., Witkowska-Pilaszewicz, O., Niewiadomska, Z., Dworecka-Kaszak, B., Ngosa Toka, F. and Jurka, P.** (2020). Role of cadherins in cancer—a review. *Int. J. Mol. Sci.* **21**, 7624. doi:10.3390/ijms21207624
- Klymenko, Y., Kim, O., Loughran, E., Yang, J., Lombard, R., Alber, M. and Stack, M. S.** (2017). Cadherin composition and multicellular aggregate invasion in organotypic models of epithelial ovarian cancer intraperitoneal metastasis. *Oncogene* **36**, 5840-5851. doi:10.1038/onc.2017.171
- Kowalczyk, A. P. and Nanes, B. A.** (2012). Adherens junction turnover: regulating adhesion through cadherin endocytosis, degradation, and recycling. *Subcell. Biochem.* **60**, 197-222. doi:10.1007/978-94-007-4186-7\_9
- Kreider-Letterman, G., Castillo, A., Mahlandt, E. K., Goedhart, J., Rabino, A., Goicoechea, S. and Garcia-Mata, R.** (2023). ARHGAP17 regulates the spatiotemporal activity of Cdc42 at invadopodia. *J. Cell Biol.* **222**, e202207020. doi:10.1083/jcb.202207020
- Kuriyama, S., Yoshida, M., Yano, S., Aiba, N., Kohno, T., Minamiya, Y., Goto, A. and Tanaka, M.** (2016). LPP inhibits collective cell migration during lung cancer dissemination. *Oncogene* **35**, 952-964. doi:10.1038/onc.2015.155
- Le, T. L., Yap, A. S. and Stow, J. L.** (1999). Recycling of E-cadherin: A potential mechanism for regulating cadherin dynamics. *J. Cell Biol.* **146**, 219-232. doi:10.1083/jcb.146.999.219
- Li, J., Fujise, K., Wint, H., Senju, Y., Suetsugu, S., Yamada, H., Takei, K. and Takeda, T.** (2021). Dynamin 2 and BAR domain protein pacsin 2 cooperatively regulate formation and maturation of podosomes. *Biochem. Biophys. Res. Commun.* **571**, 145-151. doi:10.1016/j.bbrc.2021.07.041
- Lu, Z., Ghosh, S., Wang, Z. and Hunter, T.** (2003). Downregulation of caveolin-1 function by EGF leads to the loss of E-cadherin, increased transcriptional activity of  $\beta$ -catenin, and enhanced tumor cell invasion. *Cancer Cell* **4**, 499-515. doi:10.1016/S1535-6108(03)00304-0
- Maeda, M., Johnson, K. R. and Wheelock, M. J.** (2005). Cadherin switching: essential for behavioral but not morphological changes during an epithelium-to-mesenchyme transition. *J. Cell Sci.* **118**, 873-887. doi:10.1242/jcs.01634
- Malinova, T. S., Angulo-Urarte, A., Nüchel, J., Tauber, M., van der Stoep, M. M., Janssen, V., de Haan, A., Groenen, A. G., Tebbens, M., Graupera, M. et al.** (2021). A junctional PACSIN2/EHD4/MICAL-1 complex coordinates VE-cadherin trafficking for endothelial migration and angiogenesis. *Nat. Commun.* **12**, 2610. doi:10.1038/s41467-021-22873-y
- Meng, H., Tian, L., Zhou, J., Li, Z., Jiao, X., Li, W. W., Plomann, M., Xu, Z., Lisanti, M. P., Wang, C. et al.** (2011). PACSIN 2 represses cellular migration through direct association with cyclin D1 but not its alternate splice form cyclin D1b. *Cell Cycle* **10**, 73-81. doi:10.4161/cc.10.1.14243
- Mishra, D. K., Miller, R. A., Pence, K. A. and Kim, M. P.** (2018). Small cell and non small cell lung cancer form metastasis on cellular 4D lung model. *BMC Cancer* **18**, 441. doi:10.1186/s12885-018-4358-x
- Miyashita, Y. and Ozawa, M.** (2007). Increased internalization of p120-uncoupled E-cadherin and a requirement for a dileucine motif in the cytoplasmic domain for endocytosis of the protein. *J. Biol. Chem.* **282**, 11540-11548. doi:10.1074/jbc.M608351200
- Modregger, J., Ritter, B., Witter, B., Paulsson, M. and Plomann, M.** (2000). All three PACSIN isoforms bind to endocytic proteins and inhibit endocytosis. *J. Cell Sci.* **113**, 4511-4521. doi:10.1242/jcs.113.24.4511
- Morimoto, S., Nishimura, N., Terai, T., Manabe, S., Yamamoto, Y., Shinahara, W., Miyake, H., Tashiro, S., Shimada, M. and Sasaki, T.** (2005). Rab13 mediates

- the continuous endocytic recycling of occludin to the cell surface. *J. Biol. Chem.* **280**, 2220–2228. doi:10.1074/jbc.M406906200
- Mrozik, K. M., Blaschuk, O. W., Cheong, C. M., Zannettino, A. C. W. and Vandyke, K.** (2018). N-cadherin in cancer metastasis, its emerging role in haematological malignancies and potential as a therapeutic target in cancer. *BMC Cancer* **18**, 939. doi:10.1186/s12885-018-4845-0
- Mui, K. L., Chen, C. S. and Assoian, R. K.** (2016). The mechanical regulation of integrin-cadherin crosstalk organizes cells, signaling and forces. *J. Cell Sci.* **129**, 1093–1100. doi:10.1242/jcs.183699
- Nieto, M. A., Huang, R. Y.-J., Jackson, R. A. and Thiery, J. P.** (2016). Emt: 2016. *Cell* **166**, 21–45. doi:10.1016/j.cell.2016.06.028
- Oda, H. and Takeichi, M.** (2011). Evolution: structural and functional diversity of cadherin at the adherens junction. *J. Cell Biol.* **193**, 1137–1146. doi:10.1083/jcb.201008173
- Ouyang, M., Lu, S., Kim, T., Chen, C.-E., Seong, J., Leckband, D. E., Wang, F., Reynolds, A. B., Schwartz, M. A. and Wang, Y.** (2013). N-cadherin regulates spatially polarized signals through distinct p120ctn and  $\beta$ -catenin-dependent signalling pathways. *Nat. Commun.* **4**, 1589. doi:10.1038/ncomms2560
- Pandya, P., Orgaz, J. L. and Sanz-Moreno, V.** (2017). Modes of invasion during tumour dissemination. *Mol. Oncol.* **11**, 5–27. doi:10.1002/1878-0261.12019
- Paterson, A. D., Parton, R. G., Ferguson, C., Stow, J. L. and Yap, A. S.** (2003). Characterization of E-cadherin endocytosis in isolated MCF-7 and Chinese hamster ovary cells. The initial fate of unbound E-cadherin. *J. Biol. Chem.* **278**, 21050–21057. doi:10.1074/jbc.M300082200
- Peter, B. J., Kent, H. M., Mills, I. G., Vallis, Y., Butler, P. J. G., Evans, P. R. and McMahon, H. T.** (2004). BAR domains as sensors of membrane curvature: the amphiphysin BAR structure. *Science* **303**, 495–499. doi:10.1126/science.1092586
- Pichot, C. S., Arvanitis, C., Hartig, S. M., Jensen, S. A., Bechill, J., Marzouk, S., Yu, J., Frost, J. A. and Corey, S. J.** (2010). Cdc42-interacting protein 4 promotes breast cancer cell invasion and formation of invadopodia through activation of N-WASp. *Cancer Res.* **70**, 8347–8356. doi:10.1158/0008-5472.CAN-09-4149
- Pinheiro, P. S., Jansen, A. M., de Wit, H., Tawfik, B., Madsen, K. L., Verhage, M., Gether, U. and Sorensen, J. B.** (2014). The BAR domain protein PICK1 controls vesicle number and size in adrenal chromaffin cells. *J. Neurosci.* **34**, 10688–10700. doi:10.1523/JNEUROSCI.5132-13.2014
- Plutoni, C., Bazellieres, E., Le Borgne-Rochet, M., Comunale, F., Bruges, A., Séveno, M., Planchon, D., Thuault, S., Morin, N., Bodin, S. et al.** (2016). P-cadherin promotes collective cell migration via a Cdc42-mediated increase in mechanical forces. *J. Cell Biol.* **212**, 199–217. doi:10.1083/jcb.201505105
- Qualmann, B. and Kelly, R. B.** (2000). Syndapin isoforms participate in receptor-mediated endocytosis and actin organization. *J. Cell Biol.* **148**, 1047–1062. doi:10.1083/jcb.148.5.1047
- Qualmann, B., Koch, D. and Kessels, M. M.** (2011). Let's go bananas: revisiting the endocytic BAR code. *EMBO J.* **30**, 3501–3515. doi:10.1038/emboj.2011.266
- Ratheesh, A. and Yap, A. S.** (2012). A bigger picture: classical cadherins and the dynamic actin cytoskeleton. *Nat. Rev. Mol. Cell Biol.* **13**, 673–679. doi:10.1038/nrm3431
- Ray, A., Lee, O., Win, Z., Edwards, R. M., Alford, P. W., Kim, D.-H. and Provenzano, P. P.** (2017). Anisotropic forces from spatially constrained focal adhesions mediate contact guidance directed cell migration. *Nat. Commun.* **8**, 14923. doi:10.1038/ncomms14923
- Reynolds, A. B.** (2007). p120-catenin: past and present. *Biochim. Biophys. Acta* **1773**, 2–7. doi:10.1016/j.bbamcr.2006.09.019
- Rørth, P.** (2009). Collective cell migration. *Annu. Rev. Cell Dev. Biol.* **25**, 407–429. doi:10.1146/annurev.cellbio.042308.113231
- Sabatini, P. J. B., Zhang, M., Silverman-Gavrila, R., Bendeck, M. P. and Langille, B. L.** (2008). Homotypic and endothelial cell adhesions via N-cadherin determine polarity and regulate migration of vascular smooth muscle cells. *Circ. Res.* **103**, 405–412. doi:10.1161/CIRCRESAHA.108.175307
- Safari, F. and Suetsugu, S.** (2012). The BAR domain superfamily proteins from subcellular structures to human diseases. *Membranes (Basel)* **2**, 91–117. doi:10.3390/membranes2010091
- Sánchez-Barrena, M. J., Vallis, Y., Clatworthy, M. R., Doherty, G. J., Veprintsev, D. B., Evans, P. R. and McMahon, H. T.** (2012). Bin2 is a membrane sculpting N-BAR protein that influences leucocyte podosomes, motility and phagocytosis. *PLoS ONE* **7**, e52401. doi:10.1371/journal.pone.0052401
- Schindelin, J., Arganda-Carreras, I., Frise, E., Kaynig, V., Longair, M., Pietzsch, T., Preibisch, S., Rueden, C., Saalfeld, S., Schmid, B. et al.** (2012). Fiji: an open-source platform for biological-image analysis. *Nat. Methods* **9**, 676–682. doi:10.1038/nmeth.2019
- Schneider, C. A., Rasband, W. S. and Eliceiri, K. W.** (2012). NIH Image to ImageJ: 25 years of image analysis. *Nat. Methods* **9**, 671–675. doi:10.1038/nmeth.2089
- Senju, Y., Itoh, Y., Takano, K., Hamada, S. and Suetsugu, S.** (2011). Essential role of PACSIN2/syndapin-II in caveolae membrane sculpting. *J. Cell Sci.* **124**, 2032–2040. doi:10.1242/jcs.086264
- Shellard, A. and Mayor, R.** (2021). Collective durotaxis along a self-generated stiffness gradient in vivo. *Nature* **600**, 690–694. doi:10.1038/s41586-021-04210-x
- Shih, W. and Yamada, S.** (2012). N-cadherin-mediated cell-cell adhesion promotes cell migration in a three-dimensional matrix. *J. Cell Sci.* **125**, 3661–3670. doi:10.1242/jcs.103861
- Shikanai, M., Nishimura, Y. V., Sakurai, M., Nabeshima, Y.-I., Yuzaki, M. and Kawauchi, T.** (2018). Caveolin-1 promotes early neuronal maturation via caveolae-independent trafficking of N-cadherin and L1. *iScience* **7**, 53–67. doi:10.1016/j.isci.2018.08.014
- Takeda, T., Robinson, I. M., Savoian, M. M., Griffiths, J. R., Whetton, A. D., McMahon, H. T. and Glover, D. M.** (2013). Drosophila F-BAR protein Syndapin contributes to coupling the plasma membrane and contractile ring in cytokinesis. *Open Biol.* **3**, 130081. doi:10.1098/rsob.130081
- Takei, K., Slepnev, V. I., Haucke, V. and De Camilli, P.** (1999). Functional partnership between amphiphysin and dynamin in clathrin-mediated endocytosis. *Nat. Cell Biol.* **1**, 33–39. doi:10.1038/9004
- Theveneau, E., Marchant, L., Kuriyama, S., Gull, M., Moepps, B., Parsons, M. and Mayor, R.** (2010). Collective chemotaxis requires contact-dependent cell polarity. *Dev. Cell* **19**, 39–53. doi:10.1016/j.devcel.2010.06.012
- Thiery, J. P. and Sleeman, J. P.** (2006). Complex networks orchestrate epithelial-mesenchymal transitions. *Nat. Rev. Mol. Cell Biol.* **7**, 131–142. doi:10.1038/nrm1835
- Vehlow, A., Soong, D., Vizcay-Barrena, G., Bodo, C., Law, A.-L., Perera, U. and Krause, M.** (2013). Endophilin, lamellipodin, and mena cooperate to regulate F-actin-dependent EGF-receptor endocytosis. *EMBO J.* **32**, 2722–2734. doi:10.1038/emboj.2013.212
- Wang, Y., Cao, H., Chen, J. and McNiven, M. A.** (2011). A direct interaction between the large GTPase dynamin-2 and FAK regulates focal adhesion dynamics in response to active Src. *Mol. Biol. Cell* **22**, 1529–1538. doi:10.1091/mbc.e10-09-0785
- Wang, X., Enomoto, A., Asai, N., Kato, T. and Takahashi, M.** (2016). Collective invasion of cancer: perspectives from pathology and development. *Pathol. Int.* **66**, 183–192. doi:10.1111/pin.12391
- Wheelock, M. J., Shintani, Y., Maeda, M., Fukumoto, Y. and Johnson, K. R.** (2008). Cadherin switching. *J. Cell Sci.* **121**, 727–735. doi:10.1242/jcs.000455
- Woodings, J. A., Sharp, S. J. and Machesky, L. M.** (2003). MIM-B, a putative metastasis suppressor protein, binds to actin and to protein tyrosine phosphatase delta. *Biochem. J.* **371**, 463–471. doi:10.1042/bj20021962
- Xiao, K., Allison, D. F., Buckley, K. M., Kottke, M. D., Vincent, P. A., Faundez, V. and Kowalczyk, A. P.** (2003a). Cellular levels of p120 catenin function as a set point for cadherin expression levels in microvascular endothelial cells. *J. Cell Biol.* **163**, 535–545. doi:10.1083/jcb.200306001
- Xiao, K., Allison, D. F., Kottke, M. D., Summers, S., Sorescu, G. P., Faundez, V. and Kowalczyk, A. P.** (2003b). Mechanisms of VE-cadherin processing and degradation in microvascular endothelial cells. *J. Biol. Chem.* **278**, 19199–19208. doi:10.1074/jbc.M211746200
- Yagi, T. and Takeichi, M.** (2000). Cadherin superfamily genes: functions, genomic organization, and neurologic diversity. *Genes Dev.* **14**, 1169–1180. doi:10.1101/gad.14.10.1169
- Yamada, K. M. and Sixt, M.** (2019). Mechanisms of 3D cell migration. *Nat. Rev. Mol. Cell Biol.* **20**, 738–752. doi:10.1038/s41580-019-0172-9
- Yamamoto, H., Sutoh, M., Hatakeyama, S., Hashimoto, Y., Yoneyama, T., Koie, T., Saitoh, H., Yamaya, K., Funyu, T., Nakamura, T. et al.** (2011). Requirement for FBP17 in invadopodia formation by invasive bladder tumor cells. *J. Urol.* **185**, 1930–1938. doi:10.1016/j.juro.2010.12.027
- Yang, Y., Zheng, H., Zhan, Y. and Fan, S.** (2019). An emerging tumor invasion mechanism about the collective cell migration. *Am. J. Transl. Res.* **11**, 5301–5312.
- Zhang, Y., Nolan, M., Yamada, H., Watanabe, M., Nasu, Y., Takei, K. and Takeda, T.** (2016). Dynamin2 GTPase contributes to invadopodia formation in invasive bladder cancer cells. *Biochem. Biophys. Res. Commun.* **480**, 409–414. doi:10.1016/j.bbrc.2016.10.063
- Zimu, Z., Jia, Z., Xian, F., Rui, M., Yuting, R., Yuan, W., Tianhong, W., Mian, M., Yinlong, L. and Enfang, S.** (2021). Decreased expression of PACSIN1 in brain glioma samples predicts poor prognosis. *Front. Mol. Biosci.* **8**, 696072. doi:10.3389/fmolb.2021.696072
- Zisis, T., Brückner, D. B., Brandstätter, T., Siow, W. X., d'Alessandro, J., Vollmar, A. M., Broeders, C. P. and Zahler, S.** (2022). Disentangling cadherin-mediated cell-cell interactions in collective cancer cell migration. *Biophys. J.* **1**, 44–60. doi:10.1016/j.bpj.2021.12.006

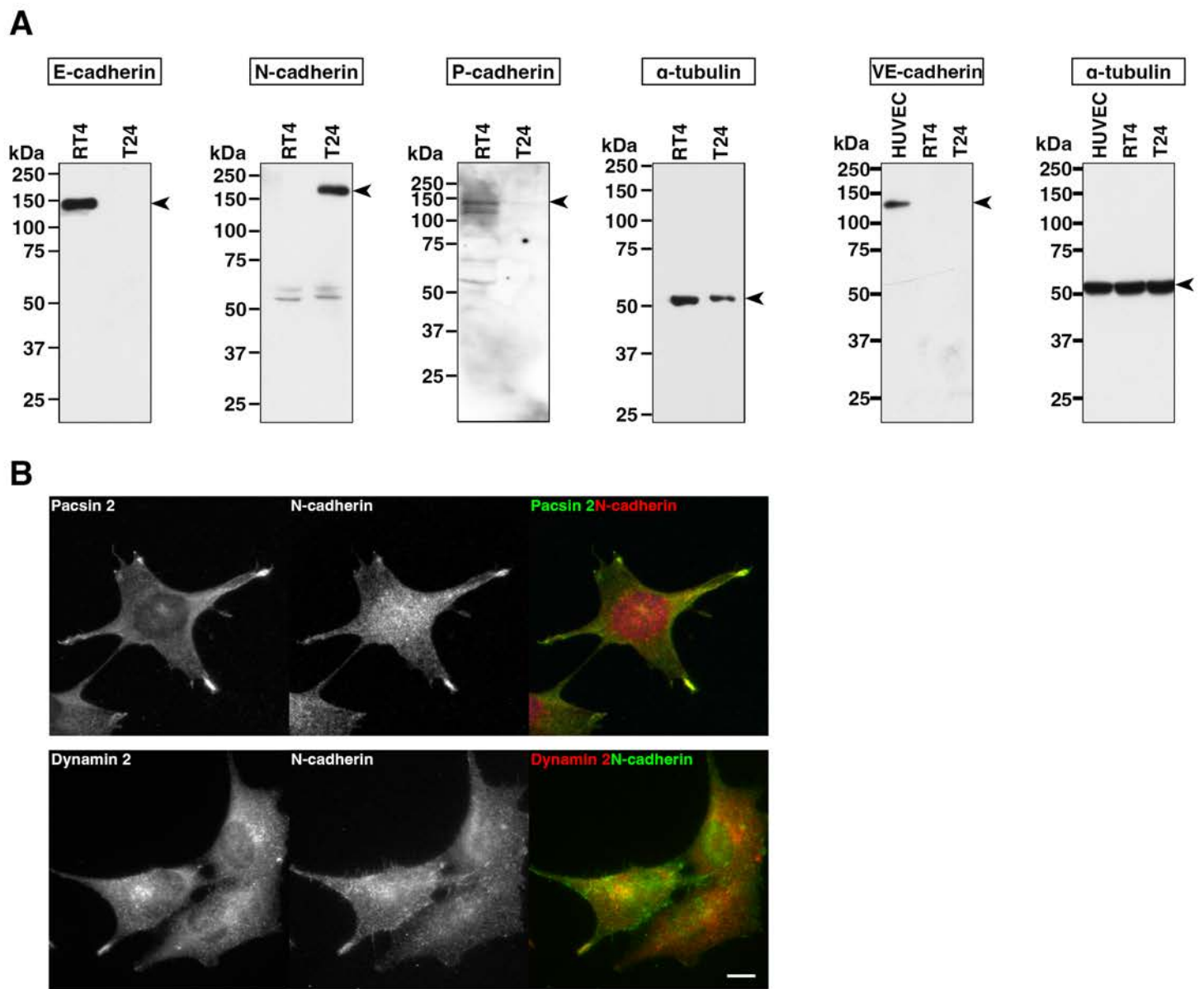
Fig. S1 Wint et al.





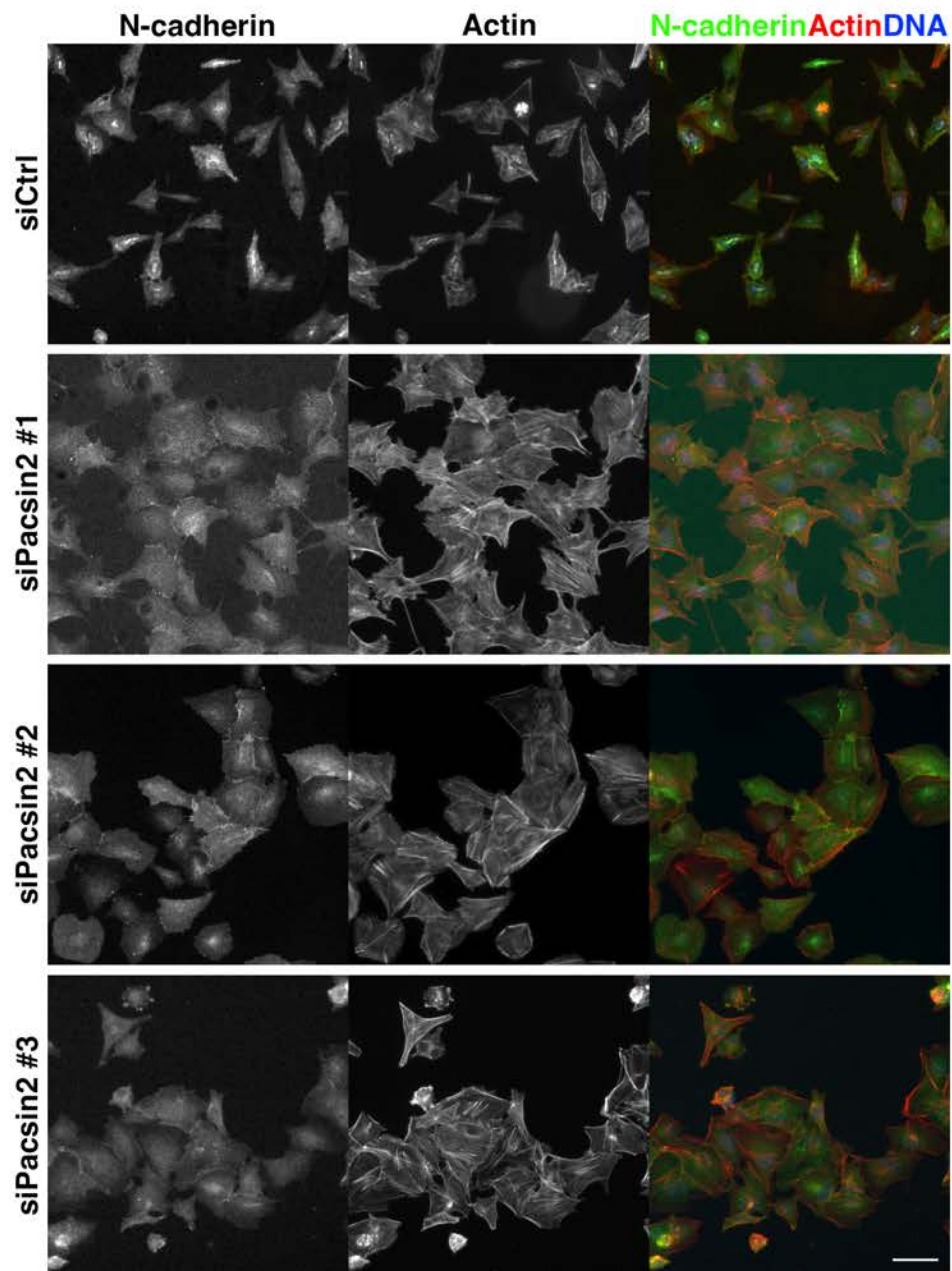
**Fig. S1. Depletion of dynamin 2 induces N-cadherin-rich bridges between contacting cells.** (A) Immunofluorescence micrographs of F-actin (red) and its merged images with DNA (blue) in control RNAi (siCtrl) or dynamin 2 RNAi (siDNM2) cells. The scale bar is 10  $\mu\text{m}$ . (B) Quantitation of the relative number of cells with cell-cell contacts for control RNAi cells (siCtrl) or dynamin 2 RNAi cells (siDNM2). Data are means  $\pm$  SD ( $n \geq 130$  cells,  $N=3$ ) (C) Immunofluorescence micrographs of control RNAi cells (siCtrl) or dynamin 2 RNAi cells (siDNM2) stained for endogenous N-cadherin (green), F-actin (red) and their merged images with DNA (blue). The scale bar is 10  $\mu\text{m}$ .

## Fig.S2 Wint et al.



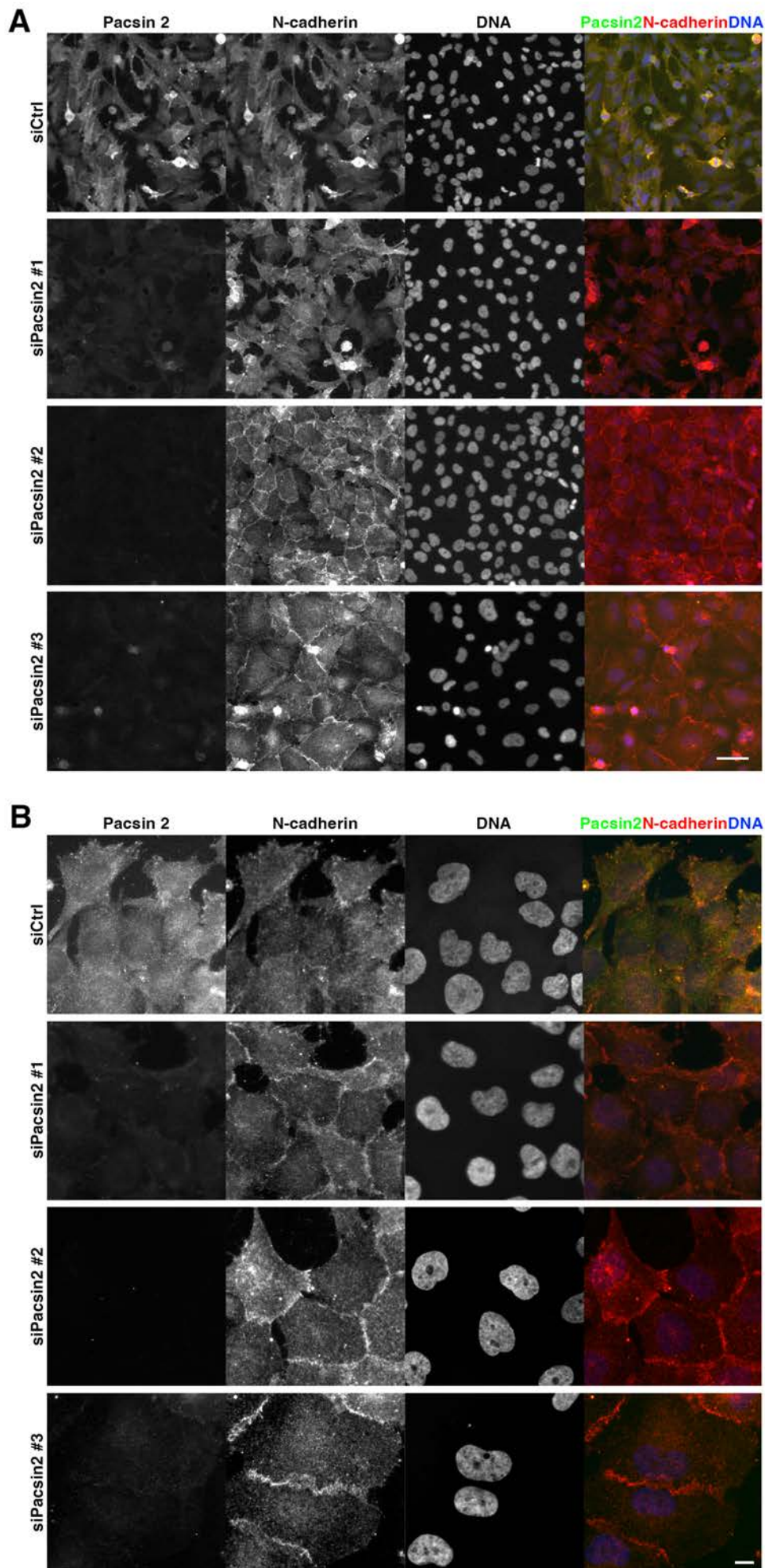
**Fig. S2. N-cadherin colocalizes with pacsin 2 and dynamin 2 at the cell periphery in T24 cells.** (A) Immunoblot analysis of endogenous E-, N- and P-cadherins in RT4 or T24 cells, and VE-cadherin in RT4, T24 or HUVEC cells together with an internal control ( $\alpha$ -tubulin). (B) Immunofluorescence micrographs of endogenous pacsin 2 (green) with endogenous N-cadherin (red) and their merged images (upper panel) or endogenous N-cadherin (green), endogenous dynamin 2 (red) and their merged images (lower panel). The scale bar is 10  $\mu$ m.

**Fig.S3 Wint et al.**



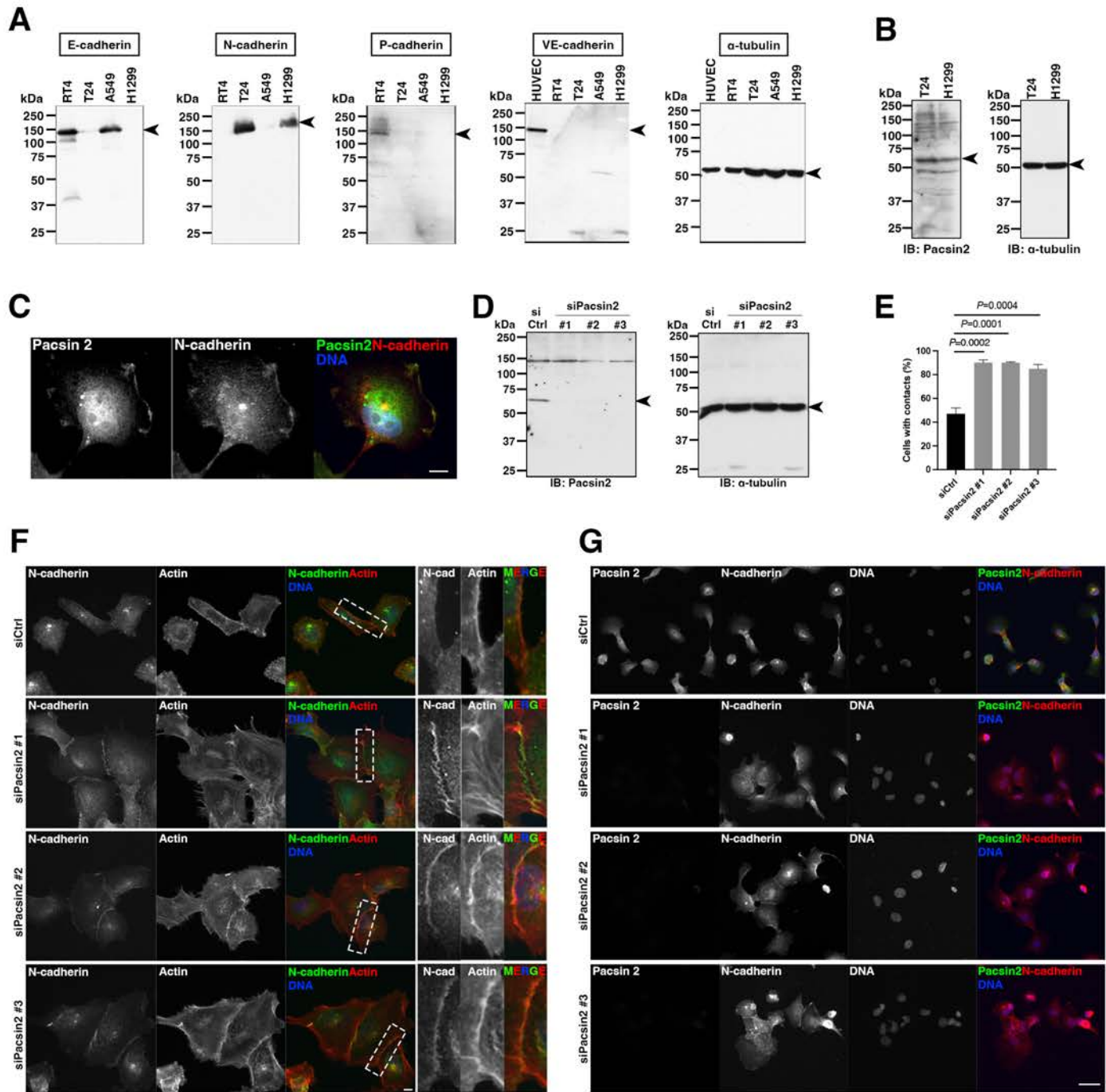
**Fig. S3. Induction of cell-cell contacts by pacsin 2 RNAi in T24 cells.** Low magnification images of N-cadherin (N-cadherin), F-actin (actin) and their merged images with DNA. The scale bar is 50  $\mu\text{m}$ .

## Fig.S4 Wint et al



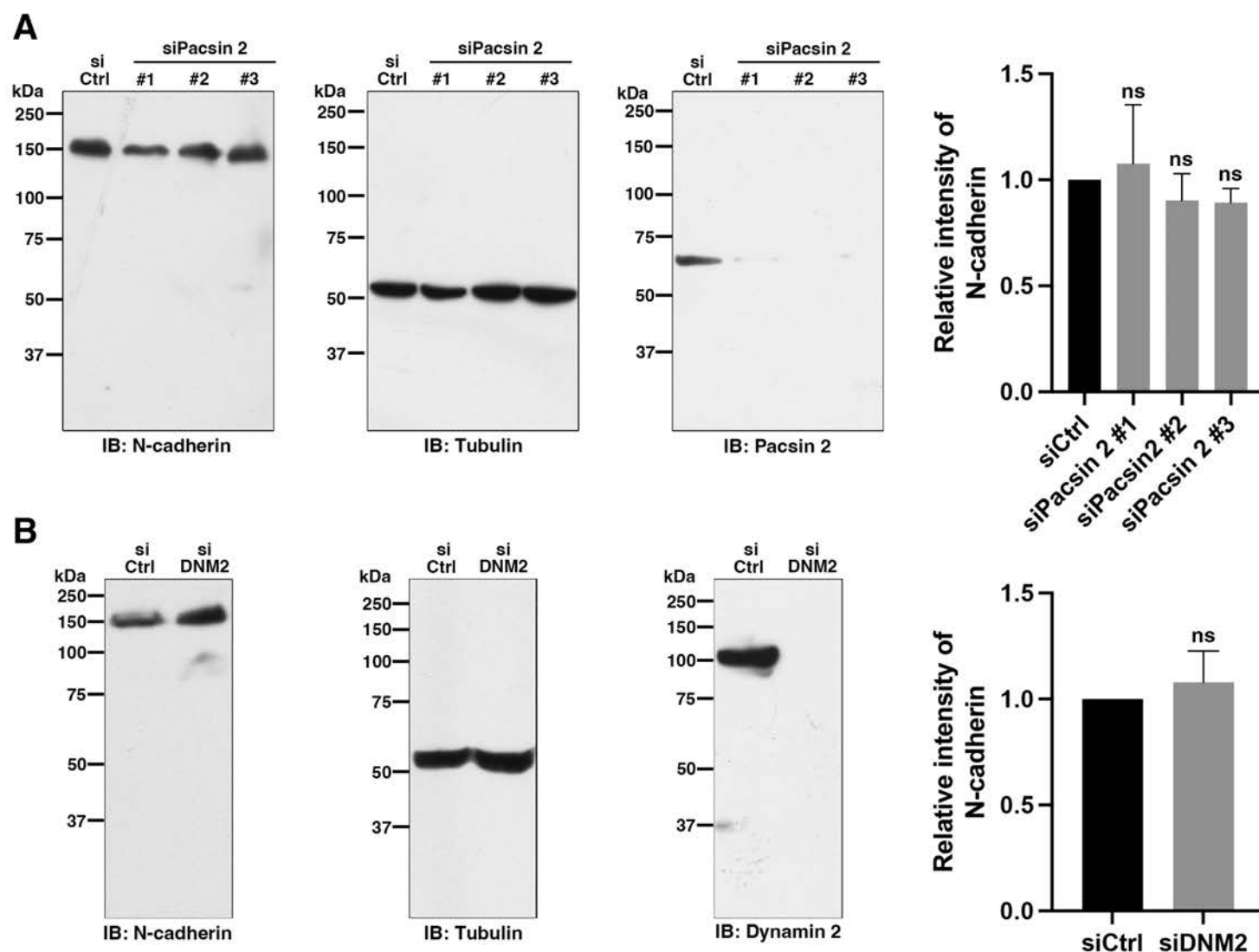
**Fig. S4 N-cadherin accumulation is induced by the depletion of pacsin 2 in T24 cells.** (A) Low and (B) high magnification immunofluorescence images of pacsin 2, N-cadherin, DNA and their merged images in control RNAi cells (siCtrl) and pacsin 2 RNAi cells (siPacsin2 #1, #2 and 3) in a densely plated condition. Scale bars are 50  $\mu$ m (A) and 10  $\mu$ m (B).

Fig. S5 Wint et al.



**Fig. S5. Depletion of pacsin 2 induces N-cadherin-rich cell junctions in H1299 cells.** (A) Expression profiles of cadherin isoforms in A549 and H1299 cells in comparison to RT4, T24 or HUVEC cells. (B) Expression of pacsin 2 in H1299 cells. Immunoblot analysis of pacsin 2 in H1299 cells in comparison to T24 is shown together with an internal control ( $\alpha$ -tubulin). (C) Immunofluorescence micrographs stained for pacsin 2 (green), N-cadherin (red) and their merged images with DNA (blue) in H1299 cells. The scale bar is 10  $\mu$ m. (D) Immunoblot analysis of cell extract from control RNAi cells (siCtrl) or pacsin 2 RNAi cells (siPacsin 2 #1, #2 and #3) using antibodies against pacsin 2 (IB: Pacsin 2) or tubulin as an internal control (IB: tubulin). (E) Depletion of pacsin 2 induces cell-cell contacts in H1299 cells. Quantitation of cells with cell contacts in control RNAi cells (siCtrl) or pacsin 2 RNAi cells (siPacsin 2 #1, #2 and #3). Data are means  $\pm$  SD ( $n \geq 229$  cells,  $N=3$ ). (F) Immunofluorescence micrographs of control RNAi cells (siCtrl) and pacsin 2 RNAi cells (siPacsin 2 #1, #2 and #3) stained for endogenous N-cadherin (green), F-actin (red) and their merged images with DNA (blue). Enlarged images show either the cell periphery in control cells or N-cadherin-rich cell-cell contact sites in pacsin 2 RNAi cells (shown in the dashed rectangle). Scale bars are 10  $\mu$ m. (G) Low magnification images of pacsin 2 (green), N-cadherin (red) and their merged images with DNA (blue). The scale bar is 50  $\mu$ m.

**Fig. S6 Wint et al.**



**Fig. S6. Expression level of N-cadherin in T24 cells is not affected by depletion of either pacsin 2 or dynamin 2.** (A) Immunoblot analyses of cell extract from either control RNAi cells (siCtrl) or pacsin 2 RNAi (siPacsin 2 #1, #2 and #3) cells using antibodies against N-cadherin (IB: N-cadherin), pacsin 2 (IB: Pacsin 2) or  $\alpha$ Tubulin (IB: Tubulin) as an internal control. Quantitation of N-cadherin levels relative to  $\alpha$ -tubulin in control RNAi cells (siCtrl) or pacsin 2 RNAi cells (siPacsin 2 #1, #2 and #3) are also shown. Data are means  $\pm$  SD (N=3) (B) Immunoblot analysis of cell extract from either control RNAi cells (siCtrl) or dynamin 2 RNAi (siDNM2) cells using antibodies against N-cadherin (IB: N-cadherin), dynamin 2 (IB: dynamin 2) or  $\alpha$ Tubulin (IB: Tubulin) as an internal control. Quantitation of N-cadherin levels relative to  $\alpha$ -tubulin in control RNAi (siCtrl) or dynamin 2 RNAi (siDNM2) cells are also shown. Data are means  $\pm$  SD (N=3).

## Fig.S7 Wint et al.

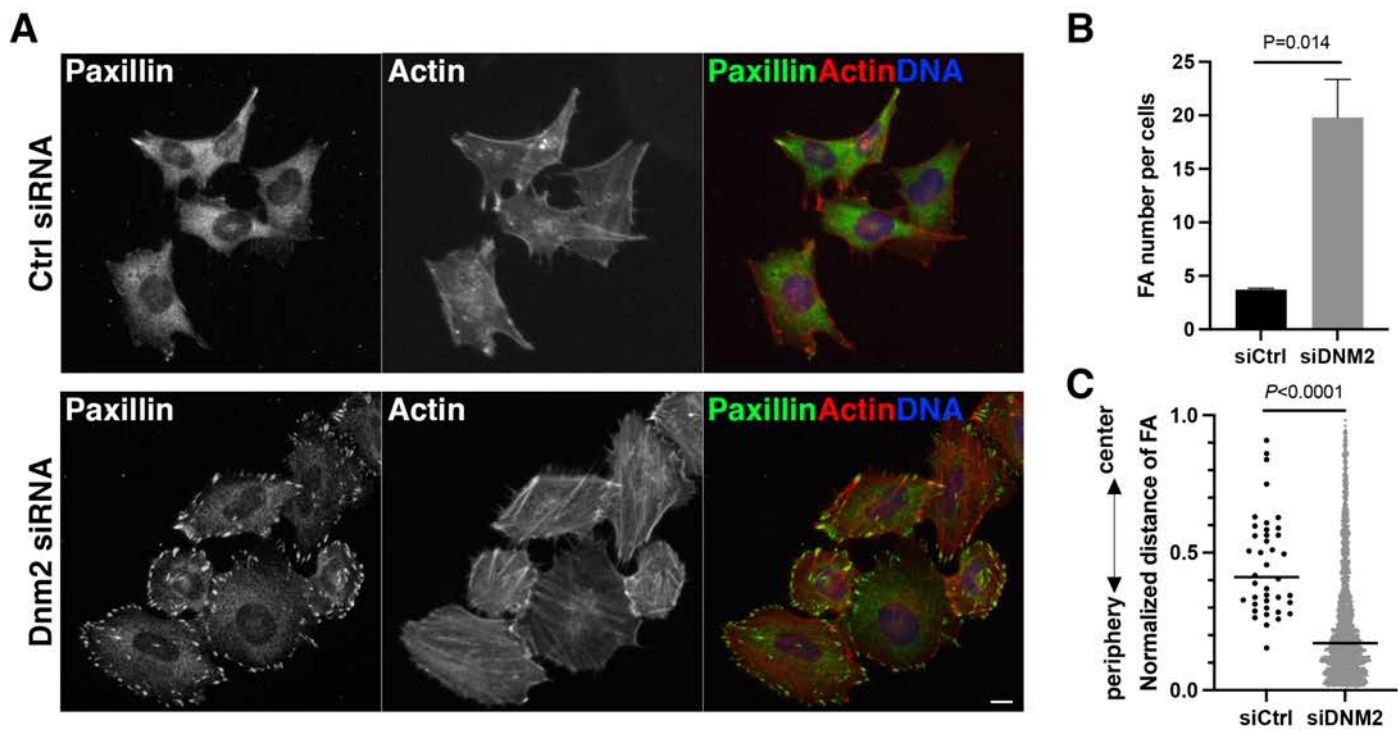


**Fig. S7. Depletion of dynamin 2 induces an elevated number of focal adhesions in T24 cells.** (A) Immunofluorescence micrographs of Paxillin (green), F-actin (red) and their merged images with DNA (blue) in control RNAi cells (siCtrl) and dynamin 2 RNAi cells (siDNM2). (B) Quantitation of focal adhesions in control RNAi cells (siCtrl) and dynamin 2 RNAi cells (siDNM2). Data are means  $\pm$  SD ( $n \geq 120$  cells,  $N=3$ ). (C) Spatial distribution of focal adhesions (FA) in either control RNAi (siCtrl) or dynamin 2 RNAi (siDNM2) cells. Normalized distance of FA between periphery (0) and centre (1) are shown (control:  $n \geq 15$  cells; siDNM2:  $n \geq 54$  cells,  $N=3$ ). The scale bar is 10  $\mu$ m.



Fig. S8 Wint et al.

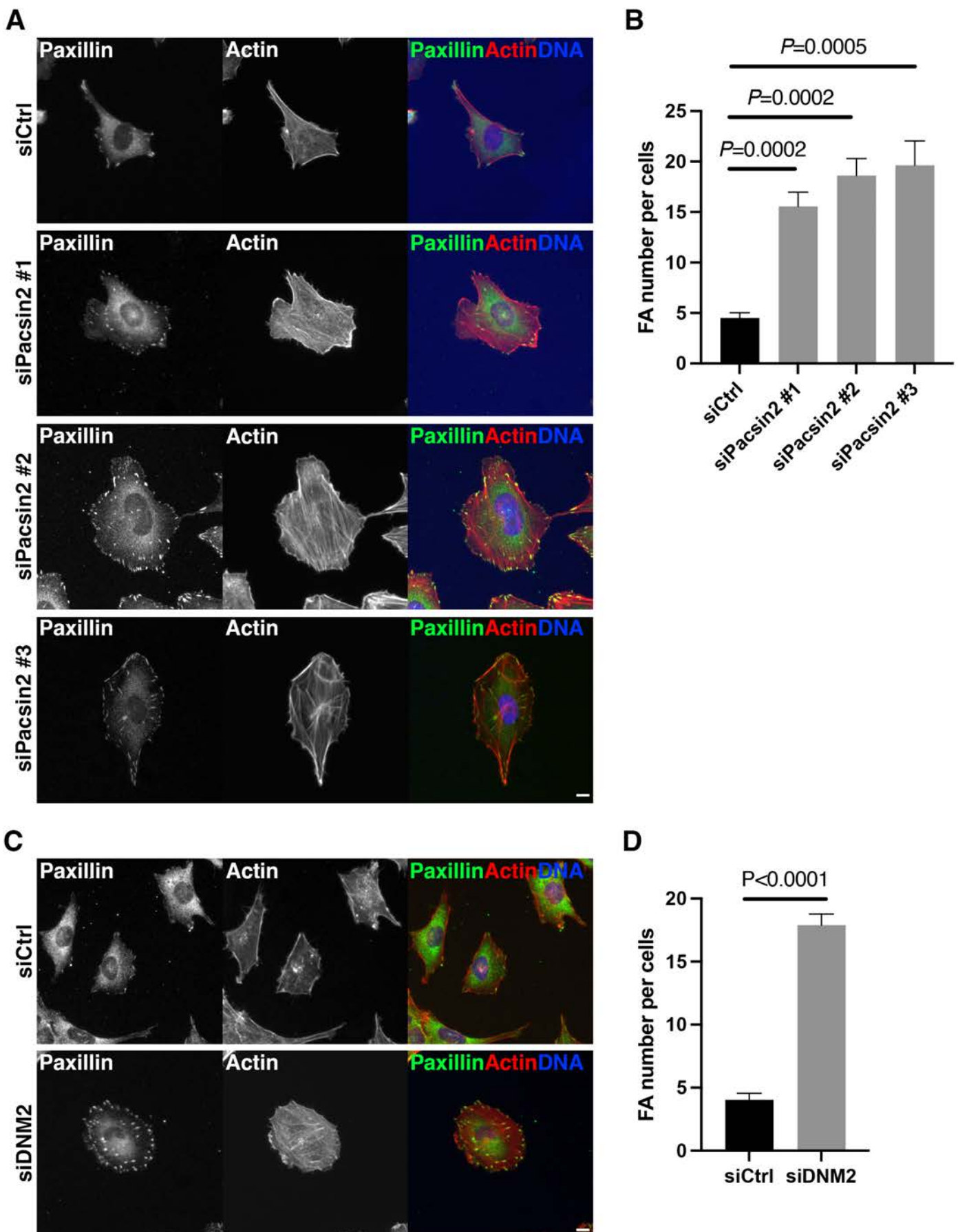


**Fig. S8. Depletion of pacsin 2 or dynamin 2 induces an elevated number of focal adhesions in single-cell conditions.** (A) Immunofluorescence micrographs of control RNAi cells (siCtrl) and pacsin 2 RNAi cells (siPacsin 2 #1, #2 and #3) stained for a focal adhesion marker paxillin (green), F-actin (red) and their merged images with DNA (blue). (B) Quantitation of focal adhesions in control RNAi cells (siCtrl) and pacsin 2 RNAi cells (siPacsin 2 #1, #2 and #3). Data are means  $\pm$  SD ( $n \geq 100$  cells,  $N=3$ ). (C) Immunofluorescence micrographs of Paxillin (green), F-actin (red) and their merged images with DNA (blue) in control RNAi cells (siCtrl) and dynamin 2 RNAi cells (siDNM2). (D) Quantitation of focal adhesions in control RNAi cells (siCtrl) and dynamin 2 RNAi cells (siDNM2). Data are means  $\pm$  SD ( $n \geq 100$  cells,  $N=3$ ).

**Table S1. Primers.**

<b>Targets</b>	<b>Primers</b>
Pacsin 2 SH3	5'-GGGG <u>ACAAGTTTGTACAAAAAAGCAGGCTGCGGGACGGAAGTGCGA</u> -3' 5'-GGGG <u>ACCACTTTGTACAAGAAAGCTGGGTTC</u> ACTGGATCGCCTCC-3'
N-cadherin Full	5'-GGGG <u>ACAAGTTTGTACAAAAAAGCAGGCTGC</u> ATGTGCCGGATAGCG-3' 5'-GGGG <u>ACCACTTTGTACAAGAAAGCTGGGT</u> CGTCATCACCTCCACCATACAT-3'
N-cadherin cytoplasmic domain	5'- <u>CACCATGAAACGCCGGGATAAAG</u> -3' 5'-TCAGTCATCACCTCCACC-3'
N-cadherin mutants P818/P821A	5'-GATCGGACCGCATACTGGGCCTCAGCGTGG-3' 5'-CCACGCTGAGGCCAGTATGCGGTCCGATC-3'
N-cadherin mutants P847/850/851A	5'-AGGGAGTCATATGCTGCAGCTGTGGCGTCATTGTCAGCC-3' 5'-GGCTGACAATGACGCCACAGCTGCAGCATATGACTCCCT-3'

\*Underlined sequences are for BP recombination (Pacsin 2 SH3 and N-cadherin Full) and Blunt TOPO PCR cloning (N-cadherin cytoplasmic domain).



**Movie 1. Control RNAi cells in the wound healing assay.** Images were obtained every 1min for 6 hours after the start of the wound healing assay. Trajectories of the ten representing cells are shown in different colours.



**Movie 2. Pacsin 2 RNAi cells in the wound healing assay.** Images were obtained every 1min for 6 hours after the start of the wound healing assay. Trajectories of the ten representing cells are shown in different colours.